Article

Developmental Cell

Inhibition of HDAC activity directly reprograms murine embryonic stem cells to trophoblast stem cells

Graphical abstract

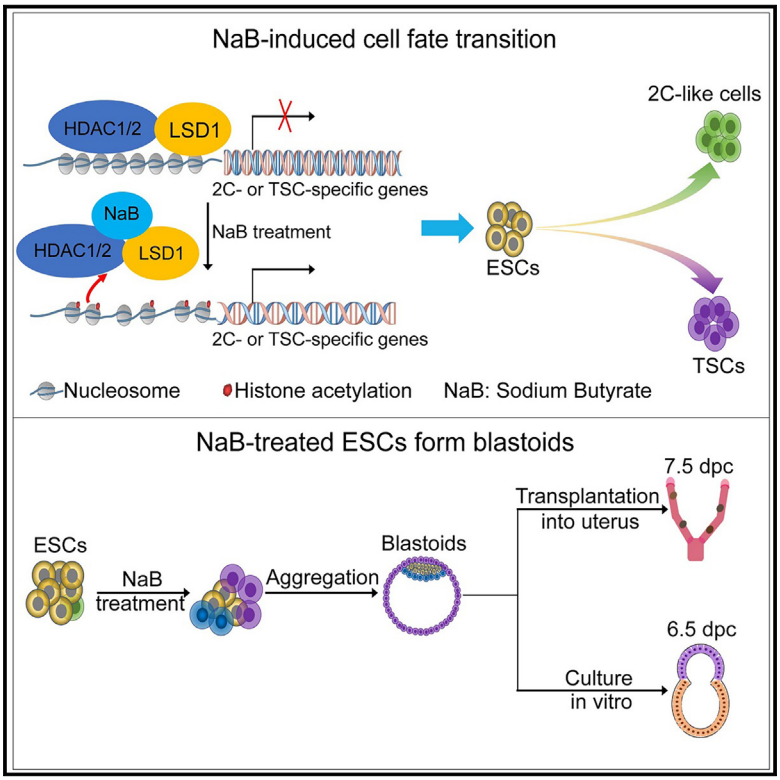

Highlights

- NaB treatment enables reprogramming of mouse ESCs into TSCs
- NaB-mediated cell reprogramming does not require a transition through a 2C-like state
- LSD1-HDAC1/2 complex represses expression of both 2C- and TSC-specific genes in ESCs
- NaB-treated ESCs readily form blastoids with the three lineages of the blastocyst

Authors

Boyan Huang, Xing Peng, Xuzhao Zhai, ..., Xiaoying Fan, Ian Chambers, Man Zhang

Correspondence

fan_xiaoying@gzlab.ac.cn (X.F.), i.chambers@ed.ac.uk (I.C.), zhang_man@gzlab.ac.cn (M.Z.)

In brief

Huang et al. find that sodium butyrate (NaB) inhibits histone deacetylase activities in the LSD1-HDAC1/2 corepressor complex to enable direct reprogramming of mouse ESCs into TSCs without a transition through a totipotent state. NaB-treated ESCs readily form blastoids containing all three cell lineages of the blastocyst.

Huang et al., 2024, Developmental Cell *59*, 1–17
August 19, 2024
https://doi.org/10.1016/j.devcel.2024.05.009

CellPress

Developmental Cell

CellPress
OPEN ACCESS

Article

Inhibition of HDAC activity directly reprograms murine embryonic stem cells to trophoblast stem cells

Boyan Huang,[1,4,9] Xing Peng,[1,9] Xuzhao Zhai,[1,4,7,9] Jie Hu,[1,4,9] Junyu Chen,[4,5] Suming Yang,[1,4] Qingpei Huang,[1] Enze Deng,[1] Huanhuan Li,[1,4] Tahsin Stefan Barakat,[6] Jiekai Chen,[3,4] Duanqing Pei,[3,8] Xiaoying Fan,[1,*] Ian Chambers,[2,*] and Man Zhang[1,4,10,*]

[1]GMU-GIBH Joint School of Life Sciences, The Fifth Affiliated Hospital of Guangzhou Medical University, Guangzhou National Laboratory, Guangzhou Medical University, Guangzhou 510005, China
[2]Centre for Regenerative Medicine, Institute for Stem Cell Research, School of Biological Sciences, University of Edinburgh, Edinburgh EH16 4UU, Scotland
[3]CAS Key Laboratory of Regenerative Biology, Guangzhou Institutes of Biomedicine and Health, Chinese Academy of Sciences, Guangzhou 510525, China
[4]Center for Cell Lineage and Atlas (CCLA), Bioland Laboratory, Guangzhou, China
[5]School of Life Science, South China Normal University, Guangzhou 510005, China
[6]Department of Clinical Genetics, Erasmus MC University Medical Center, Rotterdam, the Netherlands
[7]Zhongshan School of Medicine, Sun Yat-Sen University, Guangzhou 510080, China
[8]Present address: Laboratory of Cell Fate Control, School of Life Sciences, Westlake University, Hangzhou 310024, China
[9]These authors contributed equally
[10]Lead contact
*Correspondence: fan_xiaoying@gzlab.ac.cn (X.F.), i.chambers@ed.ac.uk (I.C.), zhang_man@gzlab.ac.cn (M.Z.)
https://doi.org/10.1016/j.devcel.2024.05.009

SUMMARY

Embryonic stem cells (ESCs) can differentiate into all cell types of the embryonic germ layers. ESCs can also generate totipotent 2C-like cells and trophectodermal cells. However, these latter transitions occur at low frequency due to epigenetic barriers, the nature of which is not fully understood. Here, we show that treating mouse ESCs with sodium butyrate (NaB) increases the population of 2C-like cells and enables direct reprogramming of ESCs into trophoblast stem cells (TSCs) without a transition through a 2C-like state. Mechanistically, NaB inhibits histone deacetylase activities in the LSD1-HDAC1/2 corepressor complex. This increases acetylation levels in the regulatory regions of both 2C- and TSC-specific genes, promoting their expression. In addition, NaB-treated cells acquire the capacity to generate blastocyst-like structures that can develop beyond the implantation stage *in vitro* and form deciduae *in vivo*. These results identify how epigenetics restrict the totipotent and trophectoderm fate in mouse ESCs.

INTRODUCTION

During embryo development, totipotent embryonic cells lose their differentiation potential and generate the inner cell mass (ICM) and the trophectoderm (TE), which represent the first events of lineage segregation.[1] Cells of the ICM will give rise to the primitive endoderm (PrE) and epiblast (EPI), the latter being the progenitor of all three germ layers of the embryo, including the germ line, whereas TE cells differentiate into the trophoblast lineages to form the placenta.[2,3] In the last decades, stem cells that capture the differentiation capacity of blastocyst cells were derived from both ICM/EPI and TE.[4,5] Pluripotent embryonic stem cells (ESCs), which originate from ICM/EPI, can differentiate into all cell types of the embryo proper but are generally excluded from the trophoblast lineage.[6] Conversely, trophoblast stem cells (TSCs) derived from the TE retain the ability to generate the trophoblast subtypes of placenta but are excluded from embryonic tissues.[5,7] ESCs and TSCs reflect the first, irrevocable cell fate decision in development, which is reinforced by distinct epigenetic lineage barriers.[8,9] Previous work showed that overexpression of a TSC-specific transcription factor, like caudal type homeobox 2 (CDX2), or repression of the pluripotency factor octamer-binding transcription factor 4 (OCT4) could differentiate mouse naive ESCs to TSC-like cells.[10,11] However, the epigenetic barriers that restrict the ESCs to TSCs transition remain largely unknown.

Interestingly, while both ESCs and TSCs lose their totipotency, there is a rare population of cells within pluripotent ESCs that express high levels of transcripts that are normally activated during the zygotic genome activation stage. These cells are referred to as 2C-like cells in mice and 8C-like cells in humans.[12–14] Transiently emerged 2C-like cells in mice can be labeled by the

Please cite this article in press as: Huang et al., Inhibition of HDAC activity directly reprograms murine embryonic stem cells to trophoblast stem cells, Developmental Cell (2024), https://doi.org/10.1016/j.devcel.2024.05.009

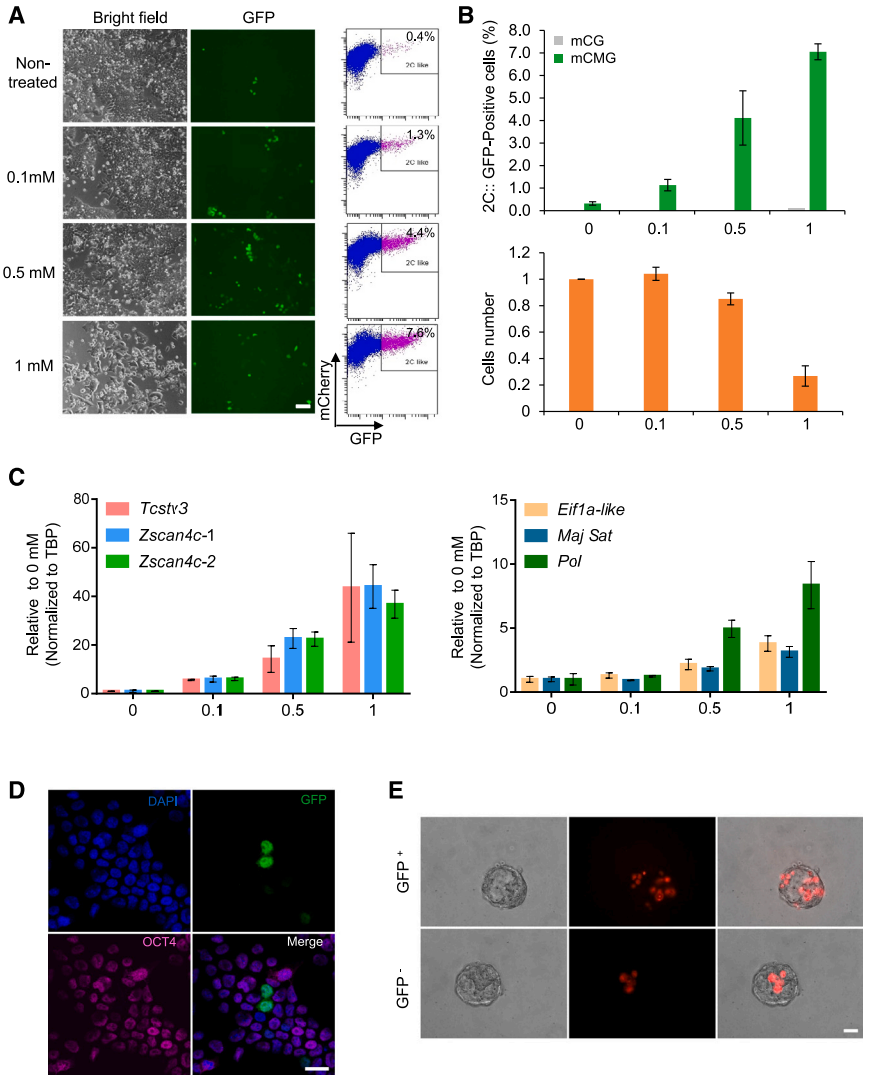

Figure 1. NaB treatment increases the proportion of 2C-like cells in ESC cultures

(A) Microscopy of mCMG1 treated with the indicated concentration of NaB. Scale bars, 50 μm; the 2C::GFP proportion is indicated (right).

(B) 2C::GFP proportion (top) and cell number (bottom) in mCG and mCMG clones treated with the indicated concentration of NaB (unit: mM) relative to non-treated control are shown. Values are means ± SD, $n = 3$ biological replicates.

(C) Quantitative mRNA analysis in mCMG clones treated with the indicated concentration of NaB (unit: mM); values are means ± SD, $n = 3$ biological replicates.

(D) Representative confocal microscopy of mCMG1 cells treated with 0.5 mM NaB for 2 days. Scale bars, 20 μm.

(E) Blastocysts generated by morula aggregation with 2C::GFP-positive cells (GFP+) and GFP-negative cells (GFP−) from 0.5 mM NaB-treated mCMG1 cell lines. Scale bars, 20 μm. See also Figures S2G and S2H.

See also Figure S1.

activity of murine endogenous retrovirus with leucine tRNA primer (MuERV-L) elements. These 2C-like cells showed expanded developmental potential, which can contribute to both embryonic and extraembryonic tissues in chimeras.[12,15] However, whether these 2C-like cells can differentiate into the trophoblast lineage *in vitro* to circumvent the epigenetic barrier between ESCs and TSCs is unknown.

Epigenetic regulation implemented in response to intrinsic and external stimuli results in the heritable modulation of gene activity, mainly through DNA and histone modifications without DNA sequence alteration.[16] Among histone modifications, acetylation normally favors an open chromatin structure and is associated with gene activation.[17] Histone deacetylases (HDACs) are responsible for histone acetylation removal and typically function as core components of the gene repression machines.[18,19] In this study, we show that HDAC inhibitor (HDACi) treatment not only increases the population of 2C-like cells in ESC cultures but also promotes the direct reprogramming of ESCs into TSCs without a transition through the 2C-like state. Moreover, our results show that class I HDACs function together with lysine-specific demethylase 1 (LSD1) to repress both TE and totipotent cell fate in mouse ESCs. This work strengthens our knowledge of how epigenetic mechanisms safeguard the pluripotent cell state from 2C and TE fate.

RESULTS

NaB treatment increases the population of 2C-like cells in ESC cultures

To obtain 2C-like cells, we first established 2C reporter cell lines by randomly integrating a linearized plasmid with CAG::mCherry; MERVL::GFP (mCMG) into E14Tg2a and used mCMG clone 1 (mCMG1) for the majority of our experiments.[20] A cell line using a plasmid without the MERVL element was generated as the negative control (mCG) (Figures S1A and S1B). GFP-positive cells emerged after culturing sorted GFP-negative cells from mCMG cells, but not from mCG cells (Figure S1C). Consistent with previous reports, MERVL-GFP-positive cells were detected with high expression levels of 2C-specific genes and low levels of OCT4 protein (Figures S1D and S1E).[12,21] Previous work showed that trichostatin A (TSA), an HDACi, slightly increases the 2C-like cell population in ESCs.[12,22] To generate considerable numbers of 2C-like cells, we treated mCMG and mCG ESCs with three different HDACi, including sodium butyrate (NaB), vorinostat (SAHA), and TSA. Our data showed that all three HDACi increased the percentage of GFP-positive cells in mCMG cells, but not in mCG cells, in a concentration-dependent manner (Figures 1A and S1F). Among them, NaB treatment gave the highest percentage of the GFP-positive cells and showed a subtle cell-toxic effect (Figures 1A and 1B) at a concentration of 0.5 mM. Therefore, we use NaB at 0.5 mM for the following experiments. Real-time qPCR showed that NaB treatment increased the expression levels of 2C-specific genes and

Please cite this article in press as: Huang et al., Inhibition of HDAC activity directly reprograms murine embryonic stem cells to trophoblast stem cells, Developmental Cell (2024), https://doi.org/10.1016/j.devcel.2024.05.009

CellPress
OPEN ACCESS

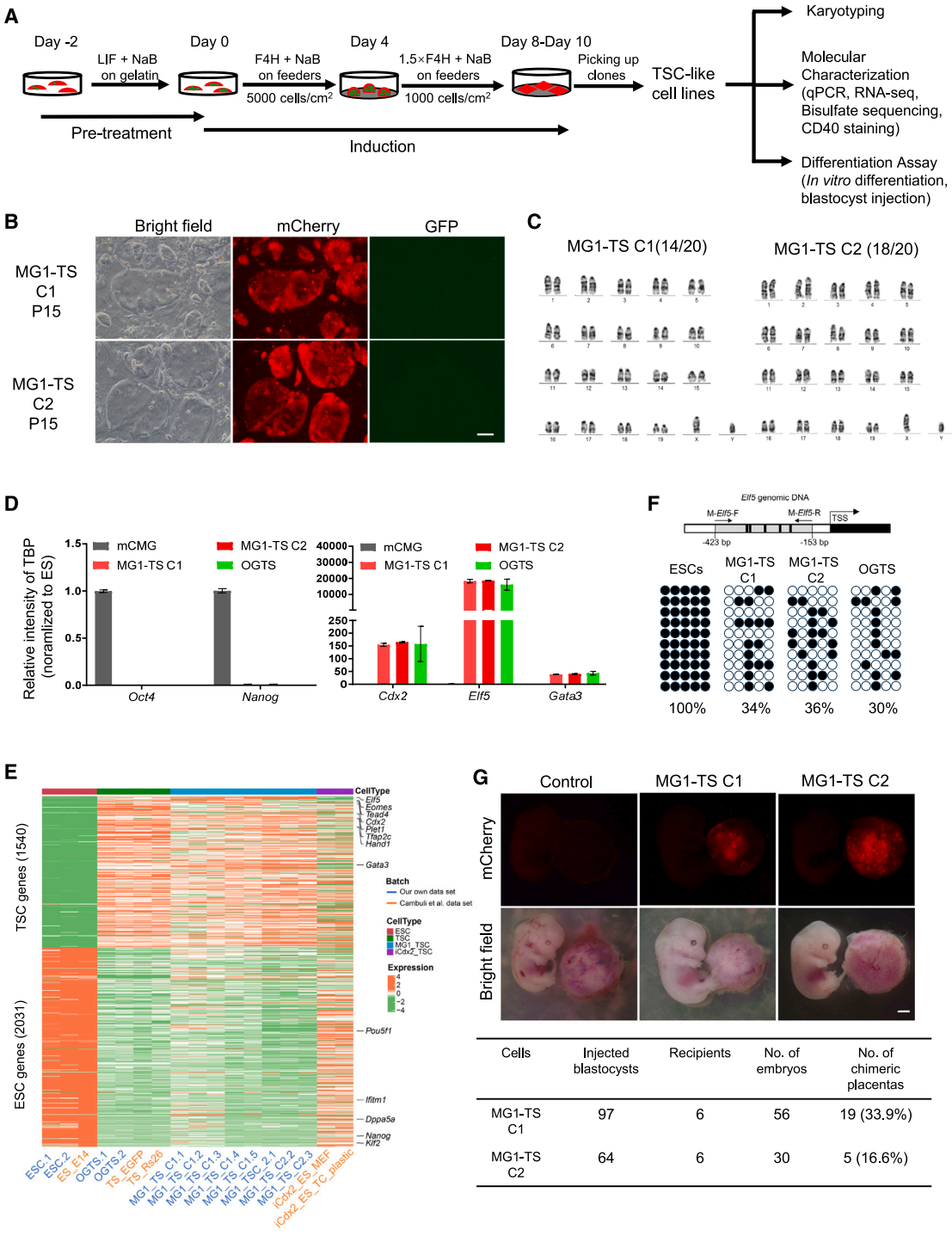

Cells	Injected blastocysts	Recipients	No. of embryos	No. of chimeric placentas
MG1-TS C1	97	6	56	19 (33.9%)
MG1-TS C2	64	6	30	5 (16.6%)

Figure 2. NaB-induced TSC-like cells from ESCs

(A) Scheme for inducing TSLCs from ESCs and the characterization of iTSLCs. F4H refers to FGF4 plus heparin.

(B) Representative microscopy images of iTSLCs (MG1-TS C1 and C2). Passage number is indicated. Scale bars, 50 μm.

(C) Karyotyping of MG1-TS C1 and C2 at the 13 passages. 20 mitotic phases in total for each cell line were analyzed. The number of cells with 40 chromosomes is indicated.

(D) Quantitative mRNA analysis in iTSLCs with mCMG1 ESCs and OGTS as control. Values are means ± SD, $n = 3$ biological replicates.

(E) Heatmap showing the differentially expressed genes between embryo-isolated OGTS versus E14Tg2a ESCs ($p \leq 0.05$, $\log_2$FC ≥ 1, the number of genes is indicated). Dataset from Cambuli et al. work (GSE62149) was labeled with orange color.[9] Key TFs implicated in TSCs and ESCs were highlighted on the right. See also Figures S2H and S2I.

(legend continued on next page)

Please cite this article in press as: Huang et al., Inhibition of HDAC activity directly reprograms murine embryonic stem cells to trophoblast stem cells, Developmental Cell (2024), https://doi.org/10.1016/j.devcel.2024.05.009

reduced OCT4 protein expression (Figures 1C and 1D). Importantly, NaB-induced GFP-positive cells can contribute to both EPI and TE lineages after aggregation with 8-cell-stage embryos (Figures 1E, S1G, and S1H).

NaB treatment transdifferentiates ESCs into TSCs

To test whether 2C-like cells can differentiate into TSCs *in vitro*, we sorted 2C::GFP-negative and 2C::GFP-positive cells from mCMG1, with or without NaB pre-treatment, and cultured them in fibroblast growth factor 4 (FGF4) plus heparin (F4H) medium on feeder cells, a condition normally used for the derivation and maintenance of TSCs.[5] After three passages in F4H, most of the GFP-positive cells became GFP-negative and showed similar morphological characteristics as the ESC clones (Figure S1I). This suggests that 2C-like cells cannot convert to TSCs *in vitro* in F4H condition. Unexpectedly, when ESCs (both mCMG1 and E14Tg2a) cultured in the F4H medium plus NaB continuously, the tight epithelial morphology of TSC-like clones, which expressed CDX2 but not NANOG, appeared after 8 days (Figures 2A, S2A, and S2B). Real-time qPCR analysis revealed that the mRNA levels of key TSC transcription factors *Cdx2*, *Elf5, Gata3*, and *Eomes* dramatically upregulated upon NaB treatment after day 0 of the induction (Figure S2C). Moreover, the proportion of cells expressing the TSC-specific surface marker CD40[23] gradually increased (Figure S2D). We then sorted CD40-positive and -negative cells and cultured them in F4H medium without NaB. After 4 days of culture, TSC-like clones appeared from CD40-positive cells and none from the CD40-negative cells (Figure S2E). To further assess the cloning efficiency of NaB-induced CD40-positive cells, we sorted 192 single CD40-positive cells at day 10 of induction into two 96-well plates in F4H medium. After 7 days, 16 TSC-like clones (16/192, 8.3%) expressing CDX2, but not OCT4, appeared. Comparatively, 51 clones (51/192, 26.6%) were formed from a single CD40-positive cell of control OCT4-GFP TSCs (OGTS), a TSC cell line established from mouse embryo (Figure S2F).[24] This result indicates that only a subpopulation of induced CD40-positive cells is capable of generating TSC-like clones. To establish stable TSC-like cell lines, we picked 25 TSC-like clones from mCMG1 cells, cultured them in TSC medium (F4H) without NaB, and successfully established 9 induced TSC-like cell (iTSLC) lines, which we referred to as MG1-TS (trophoblast stem cell) clones (Figure 2B). Two out of three clones (MG1-TS clone 1 [C1] and clone 2 [C2]) showed a normal karyotype over 13 passages (Figure 2C). We then further characterized these two clones. Similar to embryo-derived TSCs (OGTS), cells of MG1-TS C1 and C2 expressed low levels of pluripotency genes and high levels of TSC-specific genes, *Cdx2*, *Elf5*, and *Gata3* (Figure 2D), and maintained expression of TSC surface marker CD40 (Figure S2G). Moreover, high-throughput transcriptome analysis revealed that iTSLCs had similar gene expression patterns to OGTS, activating the majority of TSC-specific genes and down-regulating pluripotency genes (Figure 2E). We further compared our RNA sequencing (RNA-seq) data with those of CDX2-induced TSCs.[9] After batch correction, ESCs and embryo-derived TSCs from the two datasets matched well with each other. Notably, both PCA analysis and Pearson correlation analysis revealed that NaB-induced TSCs (MG1-TS) clustered closer with embryo-derived trophoblast cells compared with CDX2-induced TSCs (Figures S2H and S2I).[9] Besides, bisulfite sequencing revealed that the promoter regions of *Elf5* and *Tead4* in iTSLCs had comparable DNA methylation levels to those of the OGTS, and both were considerably lower than those of ESCs (Figures 2F and S2J). To evaluate the differentiation capacity of iTSLCs, iTSLCs and OGTS cells were cultured in the basal medium without feeders for *in vitro* differentiation. After 8 days of culture, the clones completely lost their epithelial morphology, and giant cells with polyploid nuclei appeared (Figure S2K). Real-time qPCR analysis revealed that differentiated cells from both iTSLCs and OGTS downregulated *Cdx2* expression and substantially increased the expression of mark genes of differentiated trophoblast subtypes, including *Syna* and *Dlx3* (expressed in labyrinth cell types), *Ascl2* and *Prl3b1* (expressed in placental junctional zone cell types), and *Prl3d1* (a marker of primary trophoblast giant cells), although with variability among the clones (Figure S2L).[10,25–29] Furthermore, we aggregated MG1-TS C1 and C2 cells with 8-cell embryos or injected them into blastocysts. Immunostaining showed that red MG1-TS cells contributed to TEs of the aggregated blastocysts, marked by the expression of CDX2 (Figure S2M). Moreover, we dissected E12.5 embryos derived from the blastocysts injected with MG1-TS cells. We observed that placentas of some embryos, but not their embryo proper, showed red fluorescence (Figure 2G). Furthermore, section immunostaining showed that mCherry-positive cells of the chimeric placenta expressed glial cells missing homolog 1 (GCM1), a marker of syncytiotrophoblast cells (Figure S2N). These results indicate that NaB-induced iTSLCs can differentiate into multiple TE lineages *in vitro* and contribute to placental development *in vivo*.

ESC-to-TSC transition occurs without a transition through a 2C-like state

Considering that NaB also increased the population of 2C-like cells, we assessed whether NaB-induced ESC to TSC (ET) transition is through the 2C-like state. We first measured the percentage of 2C::GFP-positive cells during the TSC induction. NaB increased the fraction of GFP cells to around 20% in both TSC and ESC mediums (fetal bovine serum [FBS] plus leukemia inhibitory factor [LIF]) at day 4 of induction. However, the percentage decreased dramatically (to around 3%) in the F4H medium at day 8, whereas it kept increasing (to 35%) in the ESC medium (Figures 3A and S3A–S3C). This implies that 2C::GFP cells are unable to continuously expand in F4H plus NaB medium over 4 days. To confirm this, we cultured the same number of GFP-positive and GFP-negative cells, sorted at day 4 of induction, in the F4H medium plus NaB for another 6 days (Figure 3B, left). Although clones with TSC morphology appeared from the 2C::GFP-negative cells, almost no clones survived from the

(F) Upper: scheme for the analyzed promoter region (light gray bar) of *Elf5*. Lower: DNA methylation status of indicated samples in the promoter region of *Elf5* determined by clonal bisulfite sequencing. 10 clones were analyzed for each sample. The overall percentage of methylation of each cell line is indicated.
(G) Upper: E12.5 chimeras generated by blastocyst injection with MG1-TS C1 and C2 cells, scale bars, 1 mm. Lower: summarization of embryo manipulation. See also Figure S2.

Please cite this article in press as: Huang et al., Inhibition of HDAC activity directly reprograms murine embryonic stem cells to trophoblast stem cells, Developmental Cell (2024), https://doi.org/10.1016/j.devcel.2024.05.009

CellPress
OPEN ACCESS

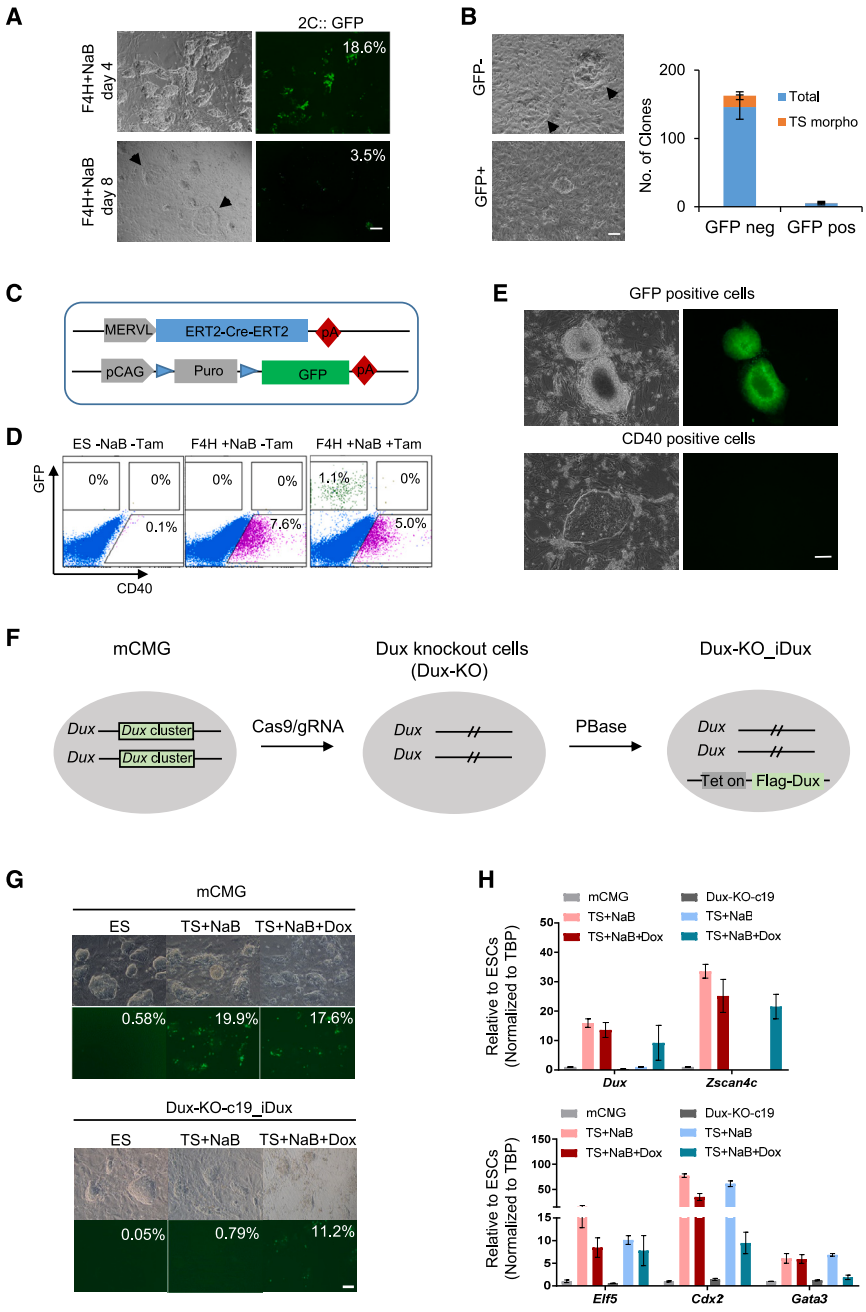

Figure 3. ESC-to-TSC transition does not require a transition through a 2C-like state

(A) Microscopy of mCMG1 cells at day 4 and day 8 of TSC induction, black arrows indicate the TSC-morphology-like clones. The 2C::GFP proportion is indicated. Scale bars, 100 μm. F4H, FGF4 plus heparin.

(B) Microscopy of GFP-negative (GFP−) and -positive (GFP+) cells that were sorted from mCMG1 at day 4 of induction and then cultured in F4H plus NaB for another 6 days, and black arrows indicate the TSC-morphology-like clones (left); scale bars, 100 μm. Quantitative analysis of clone numbers is shown (right). Values are means ± SD, *n* = 3 biological replicates.

(C) Diagram of MERVL-lineage-tracing (LT) cell line.

(D) GFP and CD40 expression analysis by fluorescence-activated cell sorting (FACS) for MERVL-LT cells at the TSC induction day 10 without (−) or with (+) 0.5 μM tamoxifen (Tam).

(E) Microscopy of sorted GFP-positive cells and CD40-positive cells cultured in F4H medium for another 4 days. Scale bars, 50 μm.

(F) Diagram of generating *Dux* knockout (KO) cells and doxycycline-induced *Dux* expression rescued cells.

(legend continued on next page)

Please cite this article in press as: Huang et al., Inhibition of HDAC activity directly reprograms murine embryonic stem cells to trophoblast stem cells, Developmental Cell (2024), https://doi.org/10.1016/j.devcel.2024.05.009

2C::GFP-positive population (Figure 3B, right). Notably, 2C-like cells are in a transient state and can spontaneously transit back into a pluripotent state under ESC culture condition in 24 h.[12,30] To further investigate whether the ET transition is through a 2C-like state, we constructed a lineage-tracing (LT) cell line to permanently label cells that had entered into the 2C-like state and referred to the cell line as MERVL-LT (Figure 3C). With ^{ERT2}Cre^{ERT2} expression driven by MERVL, 2C-like cells would express GFP permanently when tamoxifen (Tam) exists. As expected, MERVL-LT cells only showed GFP when Tam was added, and the NaB supplement increased the GFP-positive cell population (Figure S3D). Moreover, the GFP-positive cells in MERVL-LT maintained GFP expression after Tam withdrawal (Figure S3E). We then used MERVL-LT to perform the TSC induction, with or without Tam. During the induction process, the GFP-positive cell population increased when Tam was used (Figure S3F). However, at day 10 of induction with Tam, flow cytometry analysis showed that there were no CD40- and GFP-double-positive cells (Figure 3D). Moreover, in contrast to GFP-negative/CD40-positive cells, which gave rise to TSC-like clones, sorted GFP-positive cells from MERVL-LT resulted in ESCs-like clones when cultured in F4H medium (Figure 3E).

Double homeobox (DUX) is a major driver to induce the zygotic genome activation process *in vivo* and 2C-like state *in vitro*.[31–33] To further assess whether butyrate-mediated ET transition is dependent on the 2C-like state, we deleted the whole *Dux* cluster in mCMG1 ESCs and generated two *Dux* knockout (KO) clones by using Cas9 with two guide RNAs (gRNAs) (Figure S3G). As clone 13 had severe karyotypic abnormality, we used clone 19 for the rest of the experiments. We then inserted a doxycycline (Dox)-inducible construct into the Dux-KO-c19 cells to rescue *Dux* expression upon the addition of Dox (Figure 3F). We treated the cells in F4H plus NaB medium, with or without Dox, for 4 days. Consistent with previous studies,[31,32] cells without DUX (minus Dox) showed no increase in the 2C::GFP population and low mRNA levels of 2C-specific genes after the NaB treatment, while induction of DUX (plus Dox) recovered the 2C::GFP-positive cell population and increased the expression levels of 2C-specific genes in *Dux* KO cells (Figures 3G and 3H). Interestingly, *Dux* KO cells retained their ability to increase the mRNA levels of TSC-specific genes *Cdx2*, *Elf5*, and *Gata3* upon NaB treatment. In addition, the recovery of DUX showed no further enhancement of the expression of the TSC-specific genes (Figure 3H). Moreover, we established a TSC-like cell line from Dux-KO-c19 cells (Figure S3H). The Dux-KO-TSLCs showed a similar transcriptomic profile to the control TSCs (Figures S3I and S3J). These results suggest that the ET transition is a direct reprogramming event and independent of a 2C-like state.

Single-cell RNA analysis of the NaB-mediated ET transition

To further investigate the ET transition process, we performed single-cell RNA-seq (scRNA-seq) analysis during TSC induction. A total of 48,675 cells from eight time points were divided into 20 clusters, which could be assigned to five major different cell populations based on marker gene expression (Figures 4A, 4B, and S3K). Most of the clusters were ESCs (clusters 0, 1, 2, 3, 4, 5, 6, 8, 9, 12, 13, and 15). We noted that cells at induction day −2 and day 0 (clusters 2 and 5) are separated from those from the other days, implying a large transcriptomic perturbation following the transfer of ESCs into the F4H medium (Figures 4A and S3K). Additionally, we identified pre-2Cs (cluster 11), which expressed both pluripotency and totipotency genes; 2C-like cells (cluster 10), which exhibited high levels of totipotency genes; and trophoblast-like cells (cluster 14) within the population. Interestingly, we also identified an extraembryonic endoderm (XEN)-like population (cluster 16) in which cells expressed XEN marker genes and a mesoderm-like population (Figure 4B). Comparing our data with the data from cells of E1.5–E7.5 natural mouse embryos further confirmed the cell identities of the NaB-induced cell populations (Figures 4C, 4D, and S3L). To assess whether the generation of trophoblast cells is through the 2C state or pre-2C state, we performed RNA velocity analysis on those clusters closely related to the cell fate transition (clusters 1, 3, 4, 6, 9, 10, 11, 12, 14, and 15). It showed that three distinct trajectories separately branched into the 2C (cluster 10), TSC (cluster 14), and PS/mesoderm lineages (cluster 4) (Figures 4E, S3M, and S3N). Moreover, we performed pseudotime analysis using monocle 2, which showed a clearer trajectory of cell differentiation. As expected, the ESCs switched to 2C and trophoblast in two independent branches, and the cell fate was pre-determined relatively early in the pseudotime (Figure 4F). These results further suggest that NaB-induced ET transition did not go through the 2C-like state or other totipotent-like states.

Class I HDACs mediate cell fate transitions

To examine whether NaB functions as HDACi rather than its additional activities beyond, we used another two pan-specific HDACIs, TSA and SAHA, to induce TSLCs. After 10 days of induction with TSA and SAHA, a comparable number of cells of mCMG1 expressed the surface marker, CD40 (Figure 5A). We then picked up the TS-like clones and established stable TSCs (Figure 5A). In mammals, there are 18 genes coding for lysine deacetylases. These HDAC enzymes can be grouped into four classes based on their similarity to known yeast HDACs.[34] NaB inhibits most class I and class IIa HDACs.[35] To further dissect which class of HDACs function in the cell fate transition, we used class-specific HDACIs to treat ESCs within F4H medium for 4 days and then analyzed the percentage of 2C::GFP cells and the mRNA levels of 2C- and TSC-specific genes. Our data showed that inhibitors for class IIa (TMP195 and LMK235)[36,37] and IIb HDAC (TH34 and Tubacin)[38,39] showed no effect on MERVL activity or the mRNA levels of 2C and TSC genes (Figures 5B and S4A). By contrast, class-I-specific inhibitors, MGCD0103[40] and MS275[41], upregulated the mRNA levels of 2C and TSC genes and increased the 2C::GFP cells population

(G) Microscopy of indicated cell lines in the ES or F4H (TS) plus NaB, without or with doxycycline (Dox) for 4 days. The GFP proportion is indicated. Three independent experiments were performed. Scale bars, 50 μm.
(H) Quantitative mRNA analysis in mCMG and Dux-KO-c19_iDux within F4H (TS) medium plus NaB, without or with doxycycline (Dox) for 4 days. Values are means ± SD, *n* = 3 biological replicates.
See also Figure S3.

Please cite this article in press as: Huang et al., Inhibition of HDAC activity directly reprograms murine embryonic stem cells to trophoblast stem cells, Developmental Cell (2024), https://doi.org/10.1016/j.devcel.2024.05.009

CellPress
OPEN ACCESS

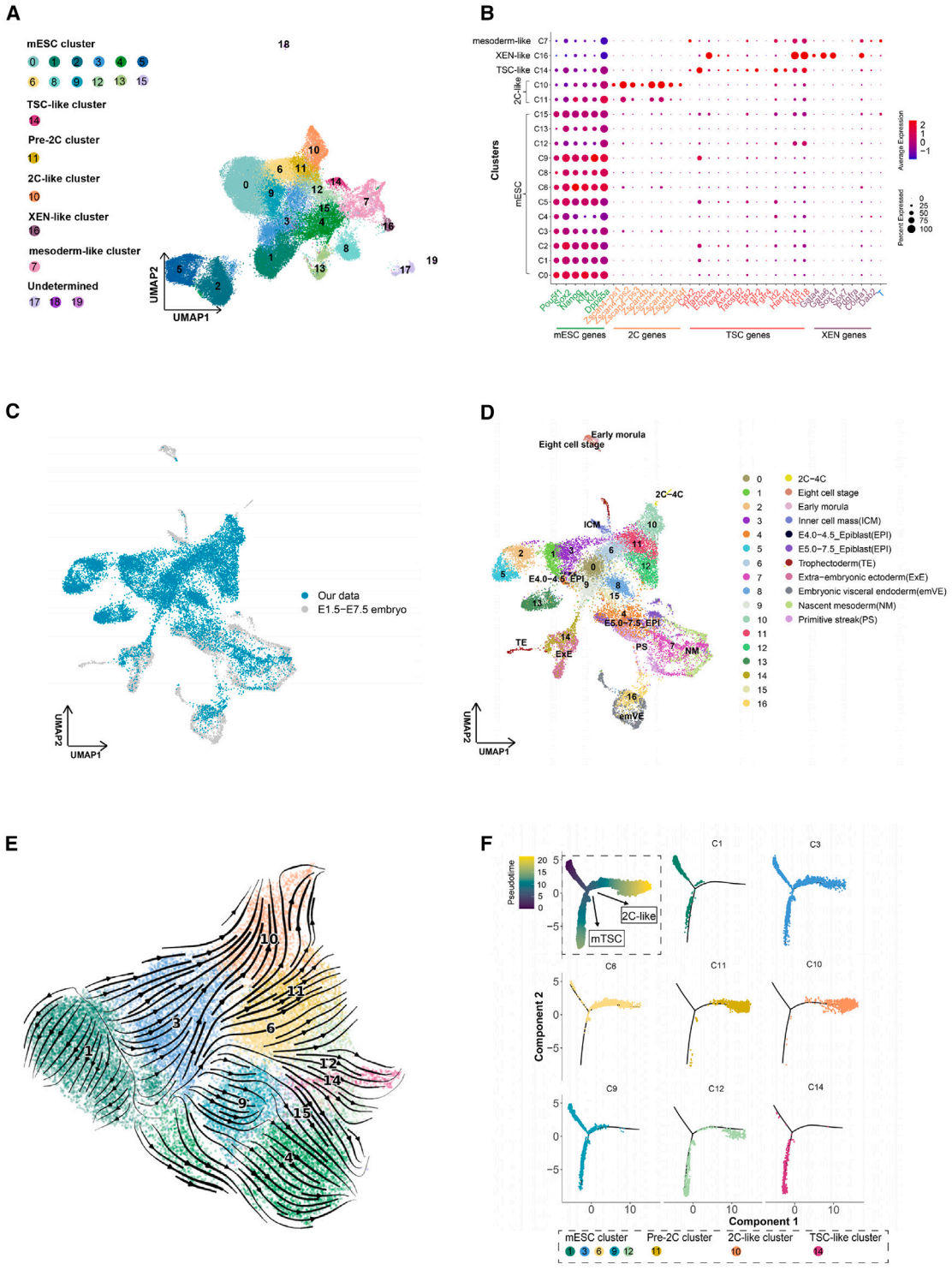

Figure 4. scRNA-seq analysis in the ET transition process

(A) Uniform manifold approximation and projection (UMAP) plot showing all cells (n = 48,675) from indicated days during NaB-mediated transdifferentiation (see Figure S3K). Cells are colored by cluster.

(B) Dotplot showing expression of cell-type-specific markers. Rows indicate cell clusters in (A).

(C and D) UMAP plot showing results of integrated analysis of scRNA-seq data from cells of the induction process and cells of the E1.5 to E7.5 natural embryo.

(legend continued on next page)

Please cite this article in press as: Huang et al., Inhibition of HDAC activity directly reprograms murine embryonic stem cells to trophoblast stem cells, Developmental Cell (2024), https://doi.org/10.1016/j.devcel.2024.05.009

in mCMG1 to a comparable level to that of NaB treatment (Figures 5B and S4A). These results suggest that it is the class I HDACs that repress 2C and TSC gene expression in ESCs. Furthermore, we used the Tam-induced *Hdac1/2* conditional double-KO (*Hdac1/2* CKO) cell line[42] to further investigate the function of class I HDACs in repressing 2C and TSC transcripts. Additionally, we introduced Dox-inducible wild-type (WT) HDAC1/2 or their catalytic activity point mutants,[43] HDAC1(H141A)/HDAC2(H142A), into the *Hdac1/2* CKO cells to rescue *Hdac1/2* expression (Figure S4B). After 3 days of culture in the F4H supplemented with Tam and Dox, we observed that cell death caused by the deletion of HDAC1/2[42] was rescued by WT HDAC1/2 but not the mutants (Figure S4C). Additionally, the expression levels of *Zscan4c*, *Dux*, and *MERVL-Pol* and *Tead4*, *Elf5*, and *Gata3* increased in the *Hdac1/2* double-KO cells. Importantly, overexpression of WT HDAC1/2, but not their point mutants, significantly diminished the upregulation of the 2C- and TSC-specific genes induced by the deletion of HDAC1/2 plus F4H (Figures 5C and S4D). These data indicate that HDAC1/2 play a major role in repressing 2C and TSC genes in ESCs.

LSD1-HDAC1/2 complex represses 2C and TSC genes in ESCs

To investigate how HDAC1/2 repress both 2C and TSC fate in ESCs, we analyzed the enrichment of the two proteins on 2C and TSC genes by using published chromatin immunoprecipitation sequencing (ChIP-seq) data in ESCs (GSE27841).[44] First, we identified 1,663 2C-up differentially expressed genes (2C-uDEGs) and 3,994 TSC-up differentially expressed genes (TSC-uDEGs), respectively, by comparing the bulk RNA-seq data of 2C-like cells and embryo-derived TSCs to the mCMG1 ESCs ($\log_2$FC > 1, adjusted $p < 0.05$) (Table S1). Both HDAC1 and HDAC2 showed enriched binding signal on the 2C and TSC uDEGs (Figures 6A and 6B). Specifically, HDAC1/2 binding regions related to 54% (900/1,663) of 2C-uDEGs and 68% (2,710/3,994) of TSC-uDEGs (Figure 6C; Table S1). To examine the effect of NaB treatment on histone acetylation modification, we first confirmed that NaB treatment increased the levels of H3K27ac and H3K9ac, the two representative markers highly correlated with active promoters and enhancers, in cells (Figure S5A). We then performed H3K27ac and H3K9ac ChIP-seq analysis in the cells at day 2 of TSC induction and compared these results with those of the untreated cells (day −2). In total, 7,314 and 10,993 differential H3K27ac and H3K9ac binding peaks were identified, respectively, with 2,905 and 8,075 peaks elevated in the NaB-treated cells. These upregulated peaks of H3K27ac or K9ac were related to 655 2C- and 1,612 TSC-uDEGs in total (Figure 6D; Table S1). Interestingly, among them, 524 2C- and 1,332 TSC-uDEGs were also bound by HDAC1 or 2 (Figures 6D and S5B). Moreover, we performed bulk RNA transcriptome analysis in the cells at induction day −2 and day 2. The differential gene analysis revealed that 4,957 genes were upregulated and 4,328 genes were downregulated upon 2 days treatment in the F4H medium plus NaB (Figure S5C; Table S2). Among them, 64.0% (1,064/1,663) of 2C-uDEGs and 38.9% (1,555/3,994) of TSC-uDEGs were activated (Figure 6E). Interestingly, 39.9% (425/1,064) of upregulated 2C-specific genes and 46.6% (724/1,555) of upregulated TSC-specific genes were related to HDAC1/2 binding-H3K27ac/K9ac upregulated peaks (Figure 6F), suggesting that those genes were potentially directly regulated by HDAC1/2.

Previous work reported that LSD1 co-precipitating with HDAC1/2 is involved in the epigenetic silencing of MERVL elements.[15,20,44] To evaluate the role of the LSD1-HDAC1/2 repressor complex in TSC transcripts repression, we analyzed published LSD1 ChIP-seq data.[44] We found that LSD1 was both enriched in the 2C and TSC genes (Figure S5D). Moreover, an average of 83% of the HDAC1/2 binding sites overlapped with LSD1 (Figure S5E), and these co-binding peaks were related to 87% of HDAC1/2 binding 2C-uDEGs and 86% of HDAC1/2 binding TSC-uDEGs (Figure S5F; Table S1). To assess whether LSD1 also represses TSC genes, we designed two short hairpin RNA (shRNA) to knock down the *Lsd1* expression in cells. Both shRNA-1 and -2 decreased the mRNA level of *Lsd1* (Figure S5G). We then induced the *Lsd1* knockdown cells within F4H plus NaB medium. This revealed that *Lsd1* repression increased mRNA levels of both 2C- and TSC-specific genes and was synergistic with NaB treatment on expression levels of TSC genes (Figure 6G). These results suggest that the LSD1-HDAC1/2 corepressor complex directly binds the regulatory regions of 2C- and TSC-specific genes to repress their expression in ESCs.

It was reported that transcription factor zinc finger, MYM-type 2 (ZMYM2) recruits the LSD1/HDAC corepressor complex to MERVL LTRs (long terminal repeats) for transcriptional repression.[15] To assess whether ZMYM2 also represses trophoblast-specific gene expression, we first analyzed published transcriptomic data.[15] Interestingly, *Zmym2* KO ESCs upregulated 2C-specific genes but downregulated TSC-specific genes (*Cdx2*, *Fgfr2*, *Hand1*, *Krt8/18*, etc.) (Figure S6A; Table S3). To further assess the function of ZMYM2 in the NaB-induced ET transition, we generated two *Zmym2* KO cell lines (Figures S6B and S6C) and treated them in F4H medium with NaB. Real-time qPCR analysis revealed that *Zmym2* KO increased the expression of 2C-specific genes but not the expression of TSC-specific genes, *Cdx2*, *Gata3*, and *Hand1* (Figure S6D). These results imply that the LSD1-HDAC1/2 repressor complex might regulate 2C- and TSC-specific genes independently by combining with different partners.

NaB-induced derepression of 2C and TSC genes occurs independent of DNA replication

Class I HDACs are also involved in histone deposition and nucleosome assembly during DNA replication for deacetylation of newly deposited histones (e.g., H4K5ac and H4K12ac)[45] and have been implicated in the maintenance of heterochromatin

(E) RNA velocity plotted onto the UMAP plot. Cells were colored by clusters in (A). Arrows indicate their estimated differentiation trends. See also Figures S3M and S3N.

(F) Single-cell trajectory analysis with cells from selected clusters using Monocle 2. The trajectory is displayed by cell clusters. Trajectory with cells colored by pseudotime is displayed in the dotted-line box.

See also Figure S3.

Please cite this article in press as: Huang et al., Inhibition of HDAC activity directly reprograms murine embryonic stem cells to trophoblast stem cells, Developmental Cell (2024), https://doi.org/10.1016/j.devcel.2024.05.009

CellPress
OPEN ACCESS

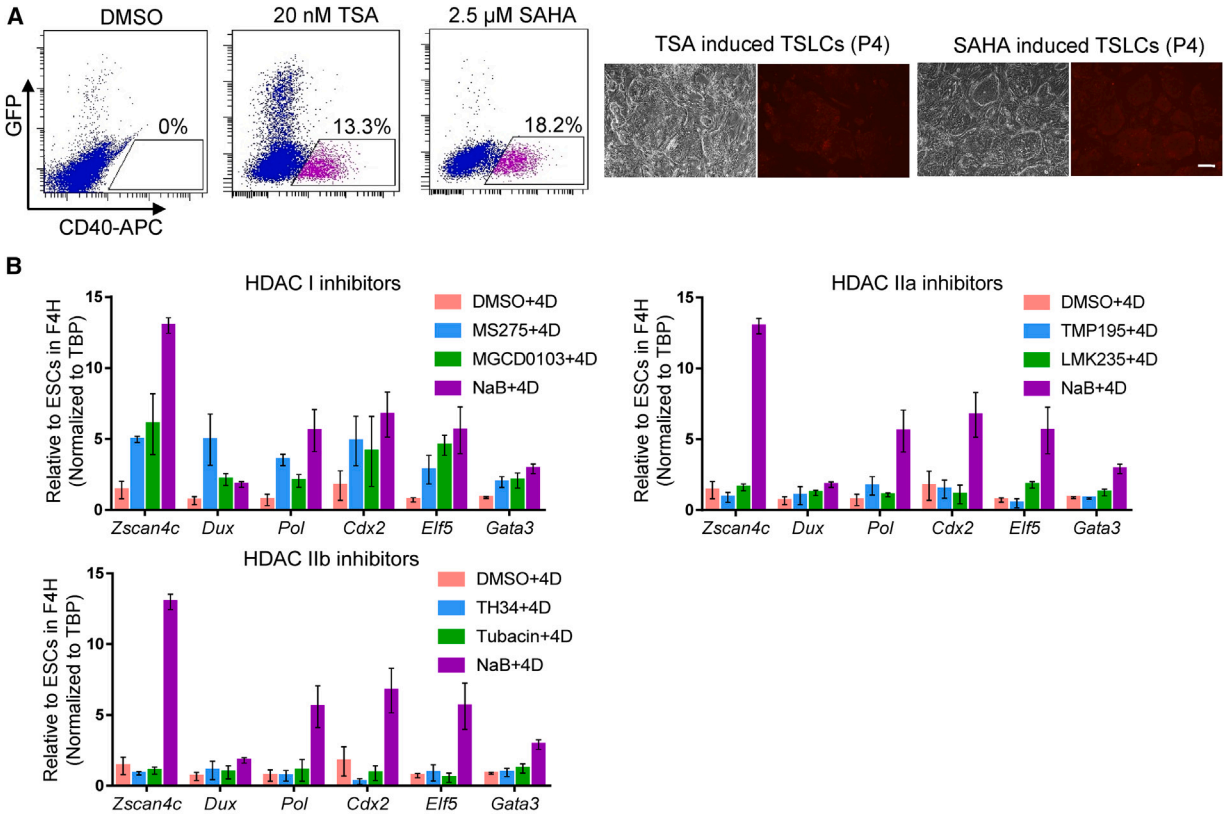

(legend on next page)

Please cite this article in press as: Huang et al., Inhibition of HDAC activity directly reprograms murine embryonic stem cells to trophoblast stem cells, Developmental Cell (2024), https://doi.org/10.1016/j.devcel.2024.05.009

domains.[46,47] To assess whether DNA replication is necessary for butyrate-induced 2C and TSC gene expression, we treated the cells with both thymidine and NaB. We first confirmed that thymidine treatment impaired DNA replication and cell mitosis (Figure S6E). Unexpectedly, flow cytometry and real-time qPCR analysis revealed that NaB treatment with thymidine still enhanced the 2C::GFP cells population and the mRNA levels of 2C and TSC marker genes (Figures S6F and S6G). These data suggest that DNA replication is dispensable for NaB-mediated derepression of 2C and TSC transcripts in ESCs.

Generation of blastocyst-like structures with NaB-treated ESCs

Previous works showed that blastocyst-like structures can be generated by aggregating cultured stem cells or totipotent-like cells.[48–51] Blastoids provide a readily accessible, tractable alternative to blastocysts for studying early embryogenesis. Our scRNA-seq data identified that cell populations with EPI, TE, and XEN transcriptional signatures existed at day 8 of induction (Figure S7A). To further assess the XEN-like population, CD140a (PDGFRa), a surface marker of PrE,[52] was used to sort the XEN-like cells at day 8 of induction (Figure S7B). CD140a-positive cells were then cultured in the medium for XEN cells to establish the XEN-like cell lines.[53] After three passages, the XEN-like cells maintained their dispersed and stellate morphology (Figure S7C). Additionally, these XEN-like cells expressed XEN marker genes but not the pluripotency genes (Figures S7D and S7E). Thereby, we hypothesize that blastoids could be generated by aggregating the NaB-treated cells at day 8 of induction. To test this hypothesis, we aggregated the MERVL-GFP-negative or -positive cells at the induction of day 8 for 5–7 days within Aggrewell in the culture condition reported for human iblastoids[54] or for extended pluripotent stem (EPS)-blastoids.[48] Interestingly, GFP-negative cells in around 11% of microwells gave rise to blastocyst-like structure with cavitation after day 6 of aggregation in the culture condition of EPS-blastoids, more than that from GFP-positive cells (Figures 7A, 7B, and S7F). Immunofluorescence revealed that blastoids from MERVL-GFP-negative cells (GFP-negative-blastoids [GN-blastoids]) expressed NANOG, CDX2, and GATA6, markers of the three cell lineages of the blastocyst, in a similar allocation to the natural embryos (Figures 7C, S7G, and S7H). Furthermore, phalloidin staining showed that the distribution of actin and adherens junctions, which was necessary to establish a barrier to enable the expansion of the blastocyst cavity,[55] was established correctly in the GN-blastoids (Figure S7I). To further determine the lineage composition and transcriptional states of the GN-blastoid cells, we performed scRNA-seq of the blastoids and compared the cells to those from E4.5 mouse embryos and the reported blastoids[48,56] (Figures 7D and S7J). This showed that the GN-blastoids contained the three cell types, ICM/EPI, TE, and PrE, which clustered to those in the blastocysts (Figure 7E) and expressed corresponding lineage-specific markers (Figures 7F and S7K). To evaluate whether the GN-blastoids could grow beyond implantation and recapitulate some aspects of post-implantation development, we cultured them in the *in vitro* culture (IVC) medium following the published method.[57] After being cultured for another 6 days, 16.2% (34/209) of blastoids and 22.4% (29/129) of blastocysts elongated and developed into egg-cylinder-like structures. Immunofluorescence showed that 25% (5/20) of the egg-cylinder-like structures from GN-blastoids and 34.5% (10/29) of those from blastocysts expressed SOX2 or OCT4 in the lower part and AP2γ (a marker of extraembryonic ectoderm) in the upper region of the egg-cylinder-like structures, surrounded by GATA6-positive cells (Figure 7G; Table S4). The onset of lumenogenesis in the post-implantation embryo relies on the repulsion of apical membranes coated by podocalyxin (PCX).[58] It was observed that 28% of natural embryos (7/25) and 28.6% (4/14) of the egg-cylinder-like structures developed from blastoids had PCX localized on the apical surface of the EPI cells, suggesting the successful polarization of the EPI cells (Figure S7L). To further evaluate the development potential of these blastoids *in vivo*, we transplanted blastoids from day 5 to day 7 into the uteri of pseudopregnant mice at 2.5 days post-coitum (dpc). We also transplanted either sesame oil or M2 solution into the uteri of pseudopregnant mice as controls. The transplanted mice were then dissected at E7.5. Although there was nothing induced from M2 solution, deciduae were induced from the sesame oil and 14.4% of the transferred blastoids (Figures 7H and S7M; Table S4). It was observed that the deciduae induced by the oil only showed vascular hubs (Figure S7N), whereas in one blastoid-induced decidua, we observed a fragment of embryo-like tissue exhibiting red fluorescence (Figure 7I). Upon section staining, it was revealed that the oil-induced deciduae did not contain any embryo tissue. By contrast, one blastoid-induced decidua (1 in 8) displayed mCherry-positive tissues expressing OCT4 and keratin 18 (KRT18), the latter being a trophoblast marker that is important for the trophoblast invasion and adhesion during embryo implantation (Figure S7O).[59] These results reveal that cells treated with NaB readily form blastocyst-like structures when aggregated *in vitro*. Additionally, a fraction of these blastoids can develop beyond implantation *in vitro* and form deciduae *in vivo*.

DISCUSSION

Our work demonstrates that the LSD1-HDAC1/2 corepressor complex represses both 2C- and TSC-specific genes in ESCs (Figure S7P). NaB treatment combined with F4H medium can directly transdifferentiate ESCs to chimera-competent TSCs.

Figure 5. Inhibition of class I HDACs derepresses 2C/TSC gene expression

(A) Left: CD40 expression analysis by FACS in mCMG1 cells treated with indicated concentrations of TSA and SAHA at day 10. Right: microscopy of established iTSLCs derived from mCMG1 by TSA (left) or SAHA (right) treatment. P4, passage number 4; scale bars, 100 μm.

(B) Quantitative mRNA analysis in mCMG1 cells with indicated inhibitor treatment for 4 days. D, days. Values are means ± SD, $n = 3$ biological replicates.

(C) Quantitative mRNA analysis in *Hdac1/2* conditional knockout cells (CKO), *Hdac1/2* wild type (WT), and point mutants' rescued cells (see Figure S4B) in the indicated culture condition, with or without tamoxifen and doxycycline (Dox) treatment, for 3 days. Values are means ± SD, $n = 3$ biological replicates. Two-sided paired t tests were performed. *$p < 0.05$; **$p < 0.01$; ***$p < 0.001$; ****$p < 0.0001$, NS, non-significant.

See also Figure S4.

Please cite this article in press as: Huang et al., Inhibition of HDAC activity directly reprograms murine embryonic stem cells to trophoblast stem cells, Developmental Cell (2024), https://doi.org/10.1016/j.devcel.2024.05.009

CellPress
OPEN ACCESS

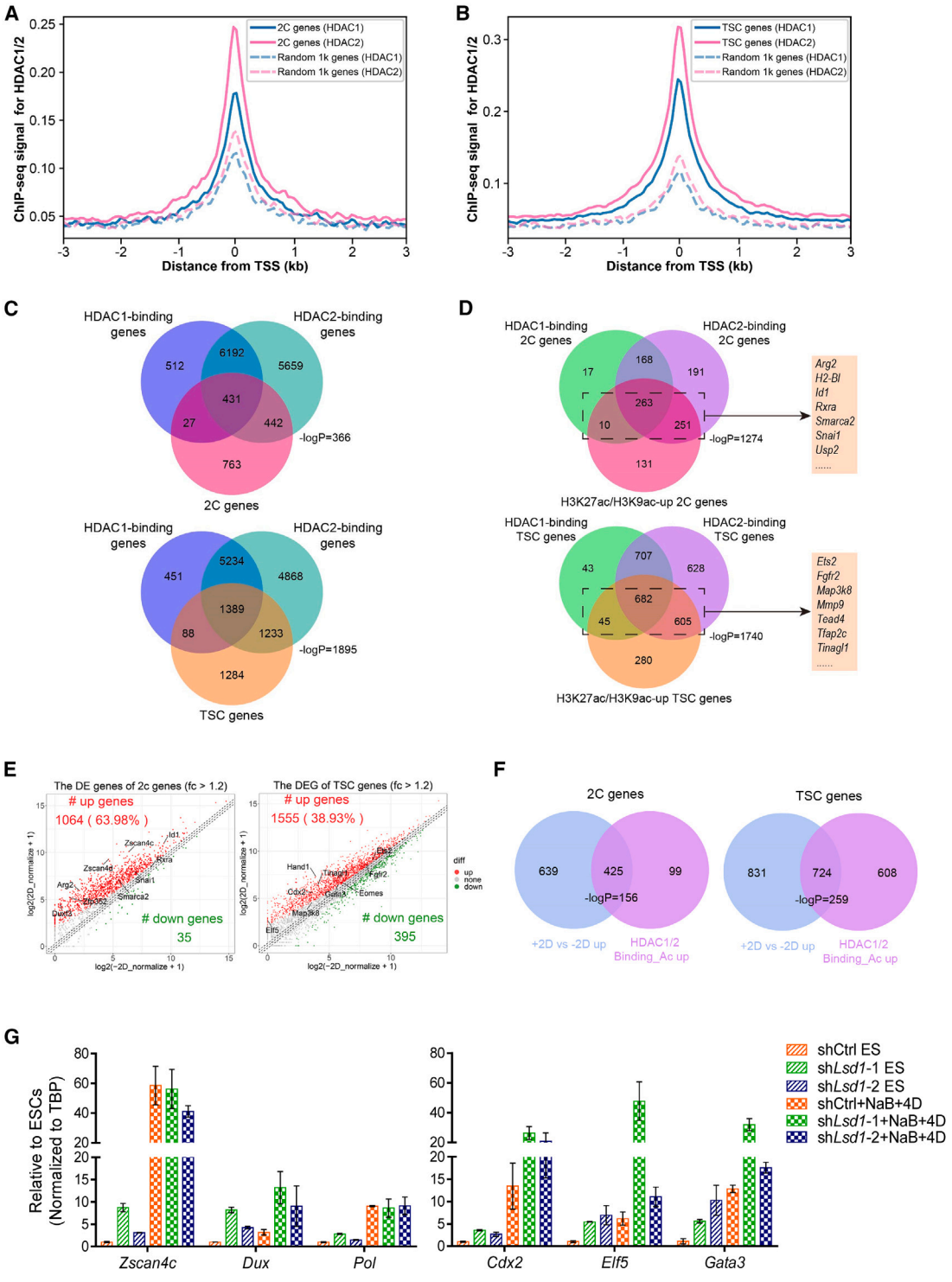

Figure 6. LSD1-HDAC1/2 repressor complex represses 2C/TSC gene expression in ESCs

(A and B) ChIP-seq signals for HDAC1 and HDAC2 in ESCs (GSE27841),[44] around TSS (±3 kb) of 2C genes (A) and TSC genes (B) compared with those of 1,000 randomly selected genes. ChIP-seq signal is represented by scores calculated using computeMatrix function in the deepTools program.

(C) Venn diagram showing overlap between HDAC1-binding genes, HDAC2-binding genes, and 2C genes (upper) or TSC genes (bottom). Hypergeometric test was performed, and the statistical *p* values were indicated.

(D) Venn diagram showing overlap between HDAC1/2-binding 2C or TSC genes and elevated H3K27ac or H3K9ac peaks, related to 2C (upper) and TSC genes (bottom). Representative genes of 2C and TSC are shown. Hypergeometric test was performed, and the statistical *p* values were indicated.

(legend continued on next page)

Please cite this article in press as: Huang et al., Inhibition of HDAC activity directly reprograms murine embryonic stem cells to trophoblast stem cells, Developmental Cell (2024), https://doi.org/10.1016/j.devcel.2024.05.009

Previous work reported that depletion of *Eset* or *Dnmt1*, which globally decreases H3K9me3, or DNA methylation in ESCs can induce some aspects of TE lineage by activating *Cdx2* or *Elf5* expression, respectively. However, these two strategies were not able to activate the full TSC transcriptome signature to establish the TSCs capable of self-renewal.[60–62] These suggest that the LSD1-HDAC1/2 complex is a predominant epigenetic factor in repressing TE fate in mouse pluripotent cells. Interestingly, recent work showed that human naive ESCs are able to readily convert to TE lineage upon the inhibition of extracelluar signal-regulated kinase (ERK)/mitogen-activated protein kinase (MAPK) and Nodal signaling. Besides, stable human TSCs could be efficiently established by culturing naive ESCs in the culture medium for human TSCs.[63,64] Evidence showed that polycomb repressive complex 2 (PRC2)-associated H3K27me3 enrichment at the promoters of trophoblast regulators in human naive stem cells ensures the extended lineage potential of the cells.[65] Further studies are required to address the decisive mechanisms underlying this epigenetic distinction across different species of mammals. Interestingly, HDACi (valproic acid [VPA]) is an important component of the human TSC medium to enhance TSC proliferation. It was also supplemented in the generation of human blastoids to support TE lineage development.[66,67] Yet, whether HDACi also promote the TE lineage transition from human naive ESCs requires further investigations.

Although 2C-like populations significantly increased during NaB-induced ET transition, our results revealed that this ET transition is independent of the 2C-like state. We showed that *Dux* KO ESCs, which blocked the activation of the 2C program, were still able to activate the TSC program after NaB treatment. Moreover, transcription factor ZMYM2, which interacts with LSD1-HDAC1/2 complex to repress the 2C program, does not repress TSC-specific genes. This implies that the LSD1-HDAC1/2 complex represses 2C- and TSC-specific genes independently, probably by combining with different partners. Our results suggested that 2C-like cells are unable to differentiate into TS-like cells *in vitro* in the F4H medium. It is noted that previous studies as well as our own have shown that 2C-like cells can contribute to both EPI and TE *in vivo* when aggregated with pre-implantation embryos.[12,15] 2C-like cells are also capable of generating blastoids with a TE-like lineage *in vitro*.[68] We think this inconsistency implies that to derive TSCs directly from 2C-like cells *in vitro* requires other signaling rather than FGF4 alone. For TE lineage specification in the embryo, position-related atypical protein kinase C (aPKC) activation mediated by Hippo signaling inhibition is important, whereas there is less positional information in a two-dimensional (2D) system. Besides, Notch signaling is also involved in the TE lineage segregation *in vivo*.[69] These signaling pathways, perhaps with other unknown signaling, might be crucial for generating TE lineage cells from 2C-like cells *in vitro* in a 2D system.

Generation of embryo-like structures *in vitro* using stem cells provides a tractable and convenient system for studying early embryogenesis. There are two main strategies for generating mouse embryo-like structures. One strategy involves aggregating cells with totipotent-like features.[48,51,68] The other strategy requires mixing three types of early embryonic lineage cells, either from cultured stem cell lines (ESCs, TSCs, and XEN) or by overexpressing determinant transcription factors for extraembryonic lineages in ESCs.[70–73] Interestingly, we showed that mouse ESCs treated with NaB and FGF4 are capable of inducing the two extraembryonic lineages and readily generating blastocyst-like structures. These blastoids contained cells with the transcriptome signatures of EPI, TE, and PrE cell types. Moreover, a small percentage of them can develop *in vitro* to recapitulate some aspects of the post-implantation development events and form decidua when transferred into the uteri of pseudopregnant mice. This supplies an alternative cell source to generate readily accessible blastoids for the investigation of mammalian early embryogenesis.

Limitations of the study

In this work, we have shown that the LSD1-HDAC1/2 complex represses both 2C- and TSC-specific genes in mouse ESCs. It is noteworthy that the ZMYM2-LSD1-HDAC1/2 complex only represses the 2C program but not the TS program. Further investigation is required to identify the potential transcription factors that interact with the LSD1-HDAC1/2 complex in ESCs to repress TSC-specific genes. Additionally, it is necessary to explore the other components that work in conjunction with the LSD1-HDAC1/2 complex to repress the expression of 2C- and/or TSC-specific genes in ESCs.

STAR★METHODS

Detailed methods are provided in the online version of this paper and include the following:

- KEY RESOURCES TABLE
- RESOURCE AVAILABILITY
  - Lead contact
  - Materials availability
  - Data and code availability
- EXPERIMENTAL MODEL AND STUDY PARTICIPANT DETAILS
  - Mice
  - Cell lines
- METHOD DETAILS
  - TSC induction
  - Establishment of XEN-like cell line
  - Lentiviral-shRNA constructions
  - Establishment of *Hdac1* and *Hdac2* inducible rescued cell lines
  - Immunostaining
  - Immunostaining of paraffin sections
  - Karyotype analysis
  - Flow cytometry (FACS)

(E) Scatterplot showing mRNA expression of differentially expressed 2C-specific genes (left) and TSC-specific genes (right) between cells at day 2 of induction (day 2) and untreated cells (day −2).
(F) Venn diagram showing overlap between upregulated genes by NaB treatment at day 2 of induction and HDAC1/2-binding-H3K27/K9ac elevated peaks related to 2C genes (left) or TSC genes (right). Hypergeometric test was performed, and the statistical *p* values were indicated.
(G) Quantitative mRNA analysis in E14Tg2a cells transfected with nonsense shRNA (shCtrl) or *Lsd1* shRNAs within F4H medium, with or without NaB, for 4 days. Values are means ± SD, *n* = 3 biological replicates.
See also Figures S5 and S6.

Please cite this article in press as: Huang et al., Inhibition of HDAC activity directly reprograms murine embryonic stem cells to trophoblast stem cells, Developmental Cell (2024), https://doi.org/10.1016/j.devcel.2024.05.009

CellPress
OPEN ACCESS

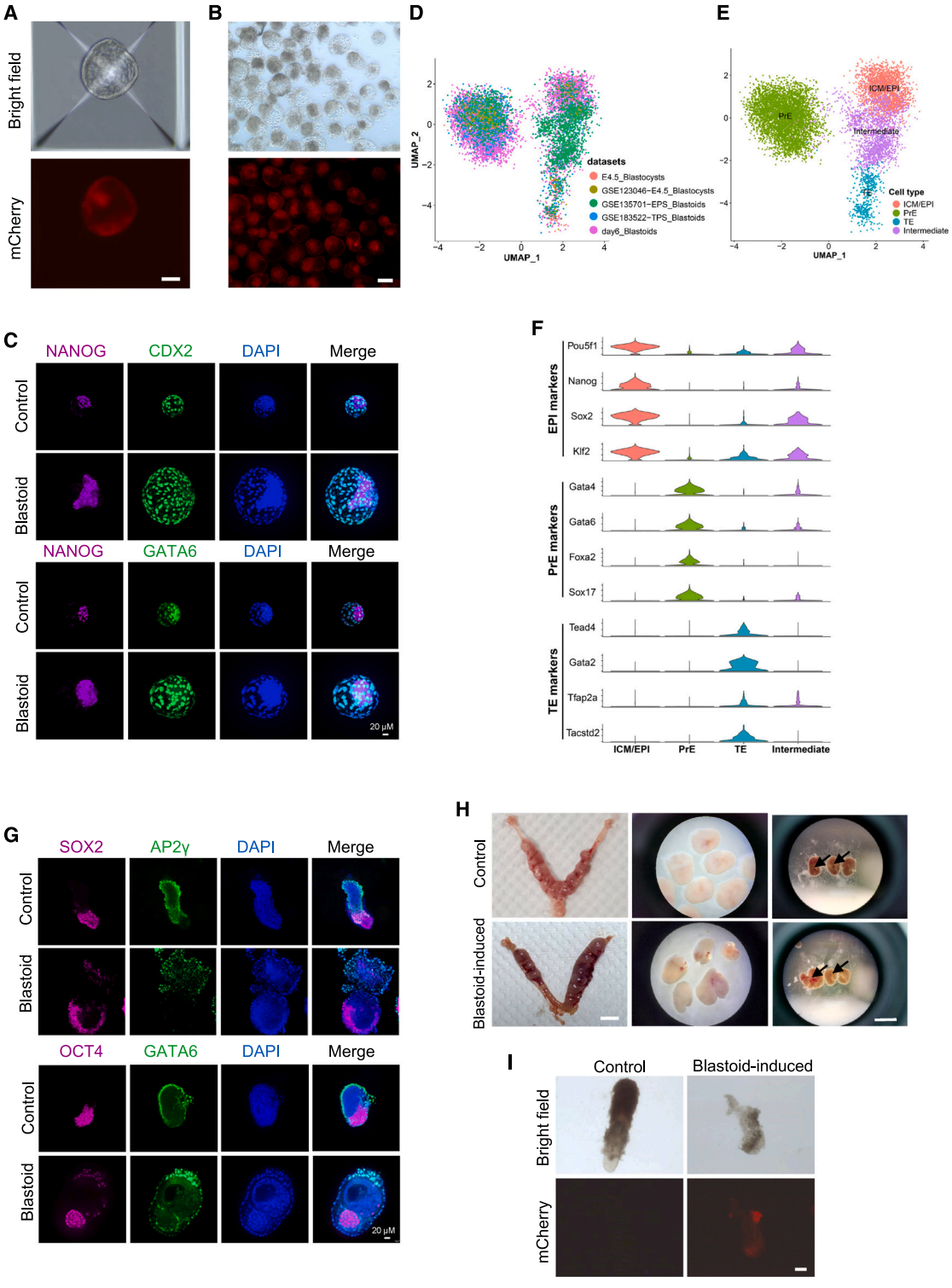

Figure 7. Generation of blastoids with cells at day 8 of TSC induction

(A and B) Microscopy of blastoids formed from GFP-negative cells in the EPS medium before (A) and after the collection (B, n = 132 blastoids from 1,200 microwells). Scale bars, 50 μm for (A) and 200 μm for (B). Experiments were performed independently at least three times (see also Figure S7F).

(C) Representative maximum projection confocal images of E3.5 blastocysts (control) and day 6 blastoids, staining for the NANOG, CDX2, and GATA6. Scale bars, 20 μm. See also Figures S7G and S7H.

(D) UMAP plot showing the results of integrated analysis of scRNA-seq data from cells of in-house and published E4.5 blastocysts[74] and indicated blastoids.[48,56]

(legend continued on next page)

- SDS–PAGE electrophoresis and immunoblotting
- RNA and qRT-PCR analysis
- Bisulfite sequencing
- Blastoids generation
- *In vitro* culture of blastocysts and blastoids
- Embryo manipulation
- Bulk RNA-seq
- ScRNA-seq
- Chromatin immunoprecipitation assay
- Bioinformatics analysis

- QUANTIFICATION AND STATISTICAL ANALYSIS

SUPPLEMENTAL INFORMATION

Supplemental information can be found online at https://doi.org/10.1016/j.devcel.2024.05.009.

ACKNOWLEDGMENTS

We thank Dr. Tilo Kunath (University of Edinburgh) for the OGTS cells and Dr. Shaun M. Cowley (University of Leicester) for the *Hdac1/2* CKO cell line. We thank Dr. Jing Liu (Guangzhou Institute of Biomedicine and Health) for the lentivirus package plasmids. We thank Dr. Jose Silva (Guangzhou National Laboratory) and Dr. Mingwei Min (Guangzhou National Laboratory) for their helpful comments about this manuscript. This work was supported by grants to M.Z. from the National Natural Science Foundation of China (grant no. 32070800), the Pearl River Talent Recruitment Program (2021ZT09Y233), and Major Project of Guangzhou National Laboratory (grant no. GZNL2023A02005).

AUTHOR CONTRIBUTIONS

I.C. and M.Z. conceived, designed, and conducted the studies; B.H., J.H., Junyu Chen, S.Y., Q.H., H.L., T.S.B., and M.Z. performed experiments; X.P., X.Z., E.D., and X.F. performed bioinformatics analysis; Jiekai Chen and D.P. provided scRNA-seq data of embryos; X.F., I.C., and M.Z. wrote the paper, with input from all authors.

DECLARATION OF INTERESTS

The authors declare no competing interests.

Received: July 11, 2023
Revised: January 23, 2024
Accepted: May 9, 2024
Published: May 31, 2024

REFERENCES

1. Dyce, J., George, M., Goodall, H., and Fleming, T.P. (1987). Do trophectoderm and inner cell mass cells in the mouse blastocyst maintain discrete lineages? Development *100*, 685–698. https://doi.org/10.1242/dev.100.4.685.
2. Fleming, T.P. (1987). A quantitative analysis of cell allocation to trophectoderm and inner cell mass in the mouse blastocyst. Dev. Biol. *119*, 520–531. https://doi.org/10.1016/0012-1606(87)90055-8.
3. Johnson, M.H., and McConnell, J.M.L. (2004). Lineage allocation and cell polarity during mouse embryogenesis. Semin. Cell Dev. Biol. *15*, 583–597. https://doi.org/10.1016/j.semcdb.2004.04.002.
4. Evans, M.J., and Kaufman, M.H. (1981). Establishment in culture of pluripotential cells from mouse embryos. Nature *292*, 154–156. https://doi.org/10.1038/292154a0.
5. Tanaka, S., Kunath, T., Hadjantonakis, A.K., Nagy, A., and Rossant, J. (1998). Promotion of trophoblast stem cell proliferation by FGF4. Science *282*, 2072–2075. https://doi.org/10.1126/science.282.5396.2072.
6. Bradley, A., Evans, M., Kaufman, M.H., and Robertson, E. (1984). Formation of germ-line chimaeras from embryo-derived teratocarcinoma cell lines. Nature *309*, 255–256. https://doi.org/10.1038/309255a0.
7. Rossant, J. (2008). Stem cells and early lineage development. Cell *132*, 527–531. https://doi.org/10.1016/j.cell.2008.01.039.
8. Reik, W. (2007). Stability and flexibility of epigenetic gene regulation in mammalian development. Nature *447*, 425–432. https://doi.org/10.1038/nature05918.
9. Cambuli, F., Murray, A., Dean, W., Dudzinska, D., Krueger, F., Andrews, S., Senner, C.E., Cook, S.J., and Hemberger, M. (2014). Epigenetic memory of the first cell fate decision prevents complete ES cell reprogramming into trophoblast. Nat. Commun. *5*, 5538. https://doi.org/10.1038/ncomms6538.
10. Blij, S., Parenti, A., Tabatabai-Yazdi, N., and Ralston, A. (2015). Cdx2Efficiently induces trophoblast stem-like cells in naïve, but not primed, pluripotent stem cells. Stem Cells Dev. *24*, 1352–1365. https://doi.org/10.1089/scd.2014.0395.
11. Niwa, H., Toyooka, Y., Shimosato, D., Strumpf, D., Takahashi, K., Yagi, R., and Rossant, J. (2005). Interaction between Oct3/4 and Cdx2 determines trophectoderm differentiation. Cell *123*, 917–929. https://doi.org/10.1016/j.cell.2005.08.040.
12. Macfarlan, T.S., Gifford, W.D., Driscoll, S., Lettieri, K., Rowe, H.M., Bonanomi, D., Firth, A., Singer, O., Trono, D., and Pfaff, S.L. (2012). Embryonic stem cell potency fluctuates with endogenous retrovirus activity. Nature *487*, 57–63. https://doi.org/10.1038/nature11244.
13. Moya-Jódar, M., Ullate-Agote, A., Barlabé, P., Rodríguez-Madoz, J.R., Abizanda, G., Barreda, C., Carvajal-Vergara, X., Vilas-Zornoza, A., Romero, J.P., Garate, L., et al. (2023). Revealing cell populations catching the early stages of human embryo development in naive pluripotent stem cell cultures. Stem Cell Rep. *18*, 64–80. https://doi.org/10.1016/j.stemcr.2022.11.015.
14. Taubenschmid-Stowers, J., Rostovskaya, M., Santos, F., Ljung, S., Argelaguet, R., Krueger, F., Nichols, J., and Reik, W. (2022). 8C-like cells capture the human zygotic genome activation program in vitro. Cell Stem Cell *29*, 449–459.e6. https://doi.org/10.1016/j.stem.2022.01.014.
15. Yang, F., Huang, X., Zang, R., Chen, J., Fidalgo, M., Sanchez-Priego, C., Yang, J., Caichen, A., Ma, F., Macfarlan, T., et al. (2020). DUX-miR-344-ZMYM2-Mediated activation of MERVL LTRs induces a totipotent 2C-like state. Cell Stem Cell *26*, 234–250.e7. https://doi.org/10.1016/j.stem.2020.01.004.
16. Bannister, A.J., and Kouzarides, T. (2011). Regulation of chromatin by histone modifications. Cell Res. *21*, 381–395. https://doi.org/10.1038/cr.2011.22.
17. Zhao, Z., and Shilatifard, A. (2019). Epigenetic modifications of histones in cancer. Genome Biol. *20*, 245. https://doi.org/10.1186/s13059-019-1870-5.
18. Dokmanovic, M., Clarke, C., and Marks, P.A. (2007). Histone deacetylase inhibitors: overview and perspectives. Mol. Cancer Res. *5*, 981–989. https://doi.org/10.1158/1541-7786.MCR-07-0324.

(E) Cell clustering results of integrated analysis in (D). Cells are colored by clusters, and cell lineage for each cluster is labeled. TE, trophectoderm; PrE, primitive endoderm; ICM/Epi, inner cell mass/epiblast.
(F) Violin plot showing expression of markers for epiblast (Epi), primitive endoderm (PrE), and trophectoderm (TE) in the cells of GN-blastoids.
(G) Representative confocal sections of E3.5 blastocysts (control) and day 6 blastoids cultured in IVC medium *in vitro* for an extra 6 days. Scale bars, 20 μm.
(H) Images of uteri (left), deciduae at E7.5 before (middle) and after (right) dissection from natural mating females (control), or pseudo-females transferred with blastoids. Scale bars, 5 mm. Black arrows indicate embryos or empty deciduae.
(I) Microscopy of E7.5 embryo and embryo-like tissue dissected from deciduae in (H). Scale bars, 200 μm.
See also Figure S7.

19. Kretsovali, A., Hadjimichael, C., and Charmpilas, N. (2012). Histone deacetylase inhibitors in cell pluripotency, differentiation, and reprogramming. Stem Cells Int. *2012*, 184154. https://doi.org/10.1155/2012/184154.

20. Macfarlan, T.S., Gifford, W.D., Agarwal, S., Driscoll, S., Lettieri, K., Wang, J., Andrews, S.E., Franco, L., Rosenfeld, M.G., Ren, B., and Pfaff, S.L. (2011). Endogenous retroviruses and neighboring genes are coordinately repressed by LSD1/KDM1A. Genes Dev. *25*, 594–607. https://doi.org/10.1101/gad.2008511.

21. Ishiuchi, T., Enriquez-Gasca, R., Mizutani, E., Bošković, A., Ziegler-Birling, C., Rodriguez-Terrones, D., Wakayama, T., Vaquerizas, J.M., and Torres-Padilla, M.E. (2015). Early embryonic-like cells are induced by downregulating replication-dependent chromatin assembly. Nat. Struct. Mol. Biol. *22*, 662–671. https://doi.org/10.1038/nsmb.3066.

22. Olbrich, T., Vega-Sendino, M., Tillo, D., Wu, W., Zolnerowich, N., Pavani, R., Tran, A.D., Domingo, C.N., Franco, M., Markiewicz-Potoczny, M., et al. (2021). CTCF is a barrier for 2C-like reprogramming. Nat. Commun. *12*, 4856. https://doi.org/10.1038/s41467-021-25072-x.

23. Rugg-Gunn, P.J., Cox, B.J., Lanner, F., Sharma, P., Ignatchenko, V., McDonald, A.C.H., Garner, J., Gramolini, A.O., Rossant, J., and Kislinger, T. (2012). Cell-surface proteomics identifies lineage-specific markers of embryo-derived stem cells. Dev. Cell *22*, 887–901. https://doi.org/10.1016/j.devcel.2012.01.005.

24. Hayakawa, K., Himeno, E., Tanaka, S., and Kunath, T. (2015). Isolation and manipulation of mouse trophoblast stem cells. Curr. Protoc. Stem Cell Biol. *32*, 1E.4.1–1E.4.32. https://doi.org/10.1002/9780470151808.sc01e04s32.

25. Simmons, D.G., Fortier, A.L., and Cross, J.C. (2007). Diverse subtypes and developmental origins of trophoblast giant cells in the mouse placenta. Dev. Biol. *304*, 567–578. https://doi.org/10.1016/j.ydbio.2007.01.009.

26. Simmons, D.G., and Cross, J.C. (2005). Determinants of trophoblast lineage and cell subtype specification in the mouse placenta. Dev. Biol. *284*, 12–24. https://doi.org/10.1016/j.ydbio.2005.05.010.

27. Tanaka, M., Gertsenstein, M., Rossant, J., and Nagy, A. (1997). Mash2 acts cell autonomously in mouse spongiotrophoblast development. Dev. Biol. *190*, 55–65. https://doi.org/10.1006/dbio.1997.8685.

28. Morasso, M.I., Grinberg, A., Robinson, G., Sargent, T.D., and Mahon, K.A. (1999). Placental failure in mice lacking the homeobox gene Dlx3. Proc. Natl. Acad. Sci. USA *96*, 162–167. https://doi.org/10.1073/pnas.96.1.162.

29. Jiang, X., Wang, Y., Xiao, Z., Yan, L., Guo, S., Wang, Y., Wu, H., Zhao, X., Lu, X., and Wang, H. (2023). A differentiation roadmap of murine placentation at single-cell resolution. Cell Discov. *9*, 30. https://doi.org/10.1038/s41421-022-00513-z.

30. Fu, X., Djekidel, M.N., and Zhang, Y. (2020). A transcriptional roadmap for 2C-like–to–pluripotent state transition. Sci. Adv. *6*, eaay5181. https://doi.org/10.1126/sciadv.aay5181.

31. De Iaco, A., Planet, E., Coluccio, A., Verp, S., Duc, J., and Trono, D. (2017). DUX-family transcription factors regulate zygotic genome activation in placental mammals. Nat. Genet. *49*, 941–945. https://doi.org/10.1038/ng.3858.

32. Hendrickson, P.G., Doráis, J.A., Grow, E.J., Whiddon, J.L., Lim, J.W., Wike, C.L., Weaver, B.D., Pflueger, C., Emery, B.R., Wilcox, A.L., et al. (2017). Conserved roles of mouse DUX and human DUX4 in activating cleavage-stage genes and MERVL/HERVL retrotransposons. Nat. Genet. *49*, 925–934. https://doi.org/10.1038/ng.3844.

33. Fu, X., Wu, X., Djekidel, M.N., and Zhang, Y. (2019). Myc and Dnmt1 impede the pluripotent to totipotent state transition in embryonic stem cells. Nat. Cell Biol. *21*, 835–844. https://doi.org/10.1038/s41556-019-0343-0.

34. Yang, X.J., and Seto, E. (2008). The Rpd3/Hda1 family of lysine deacetylases: from bacteria and yeast to mice and men. Nat. Rev. Mol. Cell Biol. *9*, 206–218. https://doi.org/10.1038/nrm2346.

35. Davie, J.R. (2003). Inhibition of histone deacetylase activity by butyrate. J. Nutr. *133*, 2485S–2493S. https://doi.org/10.1093/jn/133.7.2485S.

36. Lobera, M., Madauss, K.P., Pohlhaus, D.T., Wright, Q.G., Trocha, M., Schmidt, D.R., Baloglu, E., Trump, R.P., Head, M.S., Hofmann, G.A., et al. (2013). Selective class IIa histone deacetylase inhibition via a non-chelating zinc-binding group. Nat. Chem. Biol. *9*, 319–325. https://doi.org/10.1038/nchembio.1223.

37. Marek, L., Hamacher, A., Hansen, F.K., Kuna, K., Gohlke, H., Kassack, M.U., and Kurz, T. (2013). Histone deacetylase (HDAC) inhibitors with a novel connecting unit linker region reveal a selectivity profile for HDAC4 and HDAC5 with improved activity against chemoresistant cancer cells. J. Med. Chem. *56*, 427–436. https://doi.org/10.1021/jm301254q.

38. Butler, K.V., Kalin, J., Brochier, C., Vistoli, G., Langley, B., and Kozikowski, A.P. (2010). Rational design and simple chemistry yield a superior, neuroprotective HDAC6 inhibitor, tubastatin A. J. Am. Chem. Soc. *132*, 10842–10846. https://doi.org/10.1021/ja102758v.

39. Kolbinger, F.R., Koeneke, E., Ridinger, J., Heimburg, T., Müller, M., Bayer, T., Sippl, W., Jung, M., Gunkel, N., Miller, A.K., et al. (2018). The HDAC6/8/10 inhibitor TH34 induces DNA damage-mediated cell death in human high-grade neuroblastoma cell lines. Arch. Toxicol. *92*, 2649–2664. https://doi.org/10.1007/s00204-018-2234-8.

40. Fournel, M., Bonfils, C., Hou, Y., Yan, P.T., Trachy-Bourget, M.C., Kalita, A., Liu, J., Lu, A.H., Zhou, N.Z., Robert, M.F., et al. (2008). MGCD0103, a novel isotype-selective histone deacetylase inhibitor, has broad spectrum antitumor activity in vitro and in vivo. Mol. Cancer Ther. *7*, 759–768. https://doi.org/10.1158/1535-7163.MCT-07-2026.

41. Ryu, Y., Kee, H.J., Sun, S., Seok, Y.M., Choi, S.Y., Kim, G.R., Kee, S.J., Pflieger, M., Kurz, T., Kim, H.S., and Jeong, M.H. (2019). Class I histone deacetylase inhibitor MS-275 attenuates vasoconstriction and inflammation in angiotensin II-induced hypertension. PLoS One *14*, e0213186. https://doi.org/10.1371/journal.pone.0213186.

42. Jamaladdin, S., Kelly, R.D.W., O'Regan, L., Dovey, O.M., Hodson, G.E., Millard, C.J., Portolano, N., Fry, A.M., Schwabe, J.W.R., and Cowley, S.M. (2014). Histone deacetylase (HDAC) 1 and 2 are essential for accurate cell division and the pluripotency of embryonic stem cells. Proc. Natl. Acad. Sci. USA *111*, 9840–9845. https://doi.org/10.1073/pnas.1321330111.

43. Hassig, C.A., Tong, J.K., Fleischer, T.C., Owa, T., Grable, P.G., Ayer, D.E., and Schreiber, S.L. (1998). A role for histone deacetylase activity in HDAC1-mediated transcriptional repression. Proc. Natl. Acad. Sci. USA *95*, 3519–3524. https://doi.org/10.1073/pnas.95.7.3519.

44. Whyte, W.A., Bilodeau, S., Orlando, D.A., Hoke, H.A., Frampton, G.M., Foster, C.T., Cowley, S.M., and Young, R.A. (2012). Enhancer decommissioning by LSD1 during embryonic stem cell differentiation. Nature *482*, 221–225. https://doi.org/10.1038/nature10805.

45. Yamaguchi, T., Cubizolles, F., Zhang, Y., Reichert, N., Kohler, H., Seiser, C., and Matthias, P. (2010). Histone deacetylases 1 and 2 act in concert to promote the G1-to-S progression. Genes Dev. *24*, 455–469. https://doi.org/10.1101/gad.552310.

46. Bhaskara, S., Knutson, S.K., Jiang, G., Chandrasekharan, M.B., Wilson, A.J., Zheng, S., Yenamandra, A., Locke, K., Yuan, J.L., Bonine-Summers, A.R., et al. (2010). Hdac3 is essential for the maintenance of chromatin structure and genome stability. Cancer Cell *18*, 436–447. https://doi.org/10.1016/j.ccr.2010.10.022.

47. Sims, J.K., and Wade, P.A. (2011). Mi-2/NuRD complex function is required for normal S phase progression and assembly of pericentric heterochromatin. Mol. Biol. Cell *22*, 3094–3102. https://doi.org/10.1091/mbc.E11-03-0258.

48. Li, R., Zhong, C., Yu, Y., Liu, H., Sakurai, M., Yu, L., Min, Z., Shi, L., Wei, Y., Takahashi, Y., et al. (2019). Generation of blastocyst-like structures from mouse embryonic and adult cell cultures. Cell *179*, 687–702.e18. https://doi.org/10.1016/j.cell.2019.09.029.

49. Sozen, B., Cox, A.L., De Jonghe, J., Bao, M., Hollfelder, F., Glover, D.M., and Zernicka-Goetz, M. (2019). Self-organization of mouse stem cells into an extended potential blastoid. Dev. Cell *51*, 698–712.e8. https://doi.org/10.1016/j.devcel.2019.11.014.

50. Harrison, S.E., Sozen, B., Christodoulou, N., Kyprianou, C., and Zernicka-Goetz, M. (2017). Assembly of embryonic and extraembryonic stem cells to mimic embryogenesis in vitro. Science *356*, eaal1810. https://doi.org/10.1126/science.aal1810.

51. Zhang, P., Zhai, X., Huang, B., Sun, S., Wang, W., and Zhang, M. (2023). Highly efficient generation of blastocyst-like structures from spliceosomes-repressed mouse totipotent blastomere-like cells. Sci. China Life Sci. *66*, 423–435. https://doi.org/10.1007/s11427-022-2209-3.

52. Artus, J., Panthier, J.J., and Hadjantonakis, A.K. (2010). A role for PDGF signaling in expansion of the extra-embryonic endoderm lineage of the mouse blastocyst. Development *137*, 3361–3372. https://doi.org/10.1242/dev.050864.

53. Niakan, K.K., Schrode, N., Cho, L.T.Y., and Hadjantonakis, A.-K. (2013). Derivation of extraembryonic endoderm stem (XEN) cells from mouse embryos and embryonic stem cells. Nat. Protoc. *8*, 1028–1041. https://doi.org/10.1038/nprot.2013.049.

54. Liu, X., Tan, J.P., Schröder, J., Aberkane, A., Ouyang, J.F., Mohenska, M., Lim, S.M., Sun, Y.B.Y., Chen, J., Sun, G., et al. (2021). Modelling human blastocysts by reprogramming fibroblasts into iBlastoids. Nature *591*, 627–632. https://doi.org/10.1038/s41586-021-03372-y.

55. Zenker, J., White, M.D., Gasnier, M., Alvarez, Y.D., Lim, H.Y.G., Bissiere, S., Biro, M., and Plachta, N. (2018). Expanding actin rings zipper the mouse embryo for blastocyst formation. Cell *173*, 776–791.e17. https://doi.org/10.1016/j.cell.2018.02.035.

56. Xu, Y., Zhao, J., Ren, Y., Wang, X., Lyu, Y., Xie, B., Sun, Y., Yuan, X., Liu, H., Yang, W., et al. (2022). Derivation of totipotent-like stem cells with blastocyst-like structure forming potential. Cell Res. *32*, 513–529. https://doi.org/10.1038/s41422-022-00668-0.

57. Bedzhov, I., Leung, C.Y., Bialecka, M., and Zernicka-Goetz, M. (2014). In vitro culture of mouse blastocysts beyond the implantation stages. Nat. Protoc. *9*, 2732–2739. https://doi.org/10.1038/nprot.2014.186.

58. Bedzhov, I., and Zernicka-Goetz, M. (2014). Self-organizing properties of mouse pluripotent cells initiate morphogenesis upon implantation. Cell *156*, 1032–1044. https://doi.org/10.1016/j.cell.2014.01.023.

59. Liang, X., Qiu, X., Ma, Y., Xu, W., Chen, S., Zhang, P., Liu, M., and Lin, X. (2023). KRT18 regulates trophoblast cell migration and invasion which are essential for embryo implantation. Reprod. Biol. Endocrinol. *21*, 78. https://doi.org/10.1186/s12958-023-01129-y.

60. Ng, R.K., Dean, W., Dawson, C., Lucifero, D., Madeja, Z., Reik, W., and Hemberger, M. (2008). Epigenetic restriction of embryonic cell lineage fate by methylation of Elf5. Nat. Cell Biol. *10*, 1280–1290. https://doi.org/10.1038/ncb1786.

61. Yeap, L.S., Hayashi, K., and Surani, M.A. (2009). ERG-associated protein with SET domain (ESET)-Oct4 interaction regulates pluripotency and represses the trophectoderm lineage. Epigenetics Chromatin *2*, 12. https://doi.org/10.1186/1756-8935-2-12.

62. Yuan, P., Han, J., Guo, G., Orlov, Y.L., Huss, M., Loh, Y.H., Yaw, L.P., Robson, P., Lim, B., and Ng, H.H. (2009). Eset partners with Oct4 to restrict extraembryonic trophoblast lineage potential in embryonic stem cells. Genes Dev. *23*, 2507–2520. https://doi.org/10.1101/gad.1831909.

63. Guo, G., Stirparo, G.G., Strawbridge, S.E., Spindlow, D., Yang, J., Clarke, J., Dattani, A., Yanagida, A., Li, M.A., Myers, S., et al. (2021). Human naive epiblast cells possess unrestricted lineage potential. Cell Stem Cell *28*, 1040–1056.e6. https://doi.org/10.1016/j.stem.2021.02.025.

64. Dong, C., Beltcheva, M., Gontarz, P., Zhang, B., Popli, P., Fischer, L.A., Khan, S.A., Park, K.-M., Yoon, E.-J., Xing, X., et al. (2020). Derivation of trophoblast stem cells from naïve human pluripotent stem cells. eLife *9*, e52504. https://doi.org/10.7554/eLife.52504.

65. Kumar, B., Navarro, C., Winblad, N., Schell, J.P., Zhao, C., Weltner, J., Baqué-Vidal, L., Salazar Mantero, A., Petropoulos, S., Lanner, F., and Elsasser, S.J. (2022). Polycomb repressive complex 2 shields naive human pluripotent cells from trophectoderm differentiation. Nat. Cell Biol. *24*, 845–857. https://doi.org/10.1038/s41556-022-00916-w.

66. Okae, H., Toh, H., Sato, T., Hiura, H., Takahashi, S., Shirane, K., Kabayama, Y., Suyama, M., Sasaki, H., and Arima, T. (2018). Derivation of human trophoblast stem cells. Cell Stem Cell *22*, 50–63.e6. https://doi.org/10.1016/j.stem.2017.11.004.

67. Yu, L., Wei, Y., Duan, J., Schmitz, D.A., Sakurai, M., Wang, L., Wang, K., Zhao, S., Hon, G.C., and Wu, J. (2021). Blastocyst-like structures generated from human pluripotent stem cells. Nature *591*, 620–626. https://doi.org/10.1038/s41586-021-03356-y.

68. Yang, M., Yu, H., Yu, X., Liang, S., Hu, Y., Luo, Y., Izsvák, Z., Sun, C., and Wang, J. (2022). Chemical-induced chromatin remodeling reprograms mouse ESCs to totipotent-like stem cells. Cell Stem Cell *29*, 400–418.e13. https://doi.org/10.1016/j.stem.2022.01.010.

69. Menchero, S., Rollan, I., Lopez-Izquierdo, A., Andreu, M.J., Sainz de Aja, J., Kang, M., Adan, J., Benedito, R., Rayon, T., Hadjantonakis, A.K., and Manzanares, M. (2019). Transitions in cell potency during early mouse development are driven by Notch. eLife *8*, e42930. https://doi.org/10.7554/eLife.42930.

70. Tarazi, S., Aguilera-Castrejon, A., Joubran, C., Ghanem, N., Ashouokhi, S., Roncato, F., Wildschutz, E., Haddad, M., Oldak, B., Gomez-Cesar, E., et al. (2022). Post-gastrulation synthetic embryos generated ex utero from mouse naive ESCs. Cell *185*, 3290–3306.e25. https://doi.org/10.1016/j.cell.2022.07.028.

71. Amadei, G., Handford, C.E., Qiu, C., De Jonghe, J., Greenfeld, H., Tran, M., Martin, B.K., Chen, D.Y., Aguilera-Castrejon, A., Hanna, J.H., et al. (2022). Synthetic embryos complete gastrulation to neurulation and organogenesis. Nature *610*, 143–153. https://doi.org/10.1038/s41586-022-05246-3.

72. Sozen, B., Amadei, G., Cox, A., Wang, R., Na, E., Czukiewska, S., Chappell, L., Voet, T., Michel, G., Jing, N., et al. (2018). Self-assembly of embryonic and two extra-embryonic stem cell types into gastrulating embryo-like structures. Nat. Cell Biol. *20*, 979–989. https://doi.org/10.1038/s41556-018-0147-7.

73. Lau, K.Y.C., Rubinstein, H., Gantner, C.W., Hadas, R., Amadei, G., Stelzer, Y., and Zernicka-Goetz, M. (2022). Mouse embryo model derived exclusively from embryonic stem cells undergoes neurulation and heart development. Cell Stem Cell *29*, 1445–1458.e8. https://doi.org/10.1016/j.stem.2022.08.013.

74. Nowotschin, S., Setty, M., Kuo, Y.Y., Liu, V., Garg, V., Sharma, R., Simon, C.S., Saiz, N., Gardner, R., Boutet, S.C., et al. (2019). The emergent landscape of the mouse gut endoderm at single-cell resolution. Nature *569*, 361–367. https://doi.org/10.1038/s41586-019-1127-1.

75. Schneider, C.A., Rasband, W.S., and Eliceiri, K.W. (2012). NIH Image to ImageJ: 25 years of image analysis. Nat. Methods *9*, 671–675. https://doi.org/10.1038/nmeth.2089.

76. Kim, D., Langmead, B., and Salzberg, S.L. (2015). HISAT: a fast spliced aligner with low memory requirements. Nat. Methods *12*, 357–360. https://doi.org/10.1038/nmeth.3317.

77. Pertea, M., Pertea, G.M., Antonescu, C.M., Chang, T.C., Mendell, J.T., and Salzberg, S.L. (2015). StringTie enables improved reconstruction of a transcriptome from RNA-seq reads. Nat. Biotechnol. *33*, 290–295. https://doi.org/10.1038/nbt.3122.

78. Zhang, Y., Parmigiani, G., and Johnson, W.E. (2020). ComBat-seq: batch effect adjustment for RNA-seq count data. NAR Genom. Bioinform. *2*, lqaa078. https://doi.org/10.1093/nargab/lqaa078.

79. Ritchie, M.E., Phipson, B., Wu, D., Hu, Y., Law, C.W., Shi, W., and Smyth, G.K. (2015). limma powers differential expression analyses for RNA-sequencing and microarray studies. Nucleic Acids Res. *43*, e47. https://doi.org/10.1093/nar/gkv007.

80. Bolger, A.M., Lohse, M., and Usadel, B. (2014). Trimmomatic: a flexible trimmer for Illumina sequence data. Bioinformatics Oxf. Engl. *30*, 2114–2120. https://doi.org/10.1093/bioinformatics/btu170.

81. Dobin, A., Davis, C.A., Schlesinger, F., Drenkow, J., Zaleski, C., Jha, S., Batut, P., Chaisson, M., and Gingeras, T.R. (2013). STAR: ultrafast universal RNA-seq aligner. Bioinformatics Oxf. Engl. *29*, 15–21. https://doi.org/10.1093/bioinformatics/bts635.

82. Anders, S., Pyl, P.T., and Huber, W. (2015). HTSeq–a Python framework to work with high-throughput sequencing data. Bioinformatics Oxf. Engl. *31*, 166–169. https://doi.org/10.1093/bioinformatics/btu638.

83. Love, M.I., Huber, W., and Anders, S. (2014). Moderated estimation of fold change and dispersion for RNA-seq data with DESeq2. Genome Biol. *15*, 550. https://doi.org/10.1186/s13059-014-0550-8.

84. Stuart, T., Butler, A., Hoffman, P., Hafemeister, C., Papalexi, E., Mauck, W.M., 3rd, Hao, Y., Stoeckius, M., Smibert, P., and Satija, R. (2019). Comprehensive integration of single-cell data. Cell *177*, 1888–1902.e21. https://doi.org/10.1016/j.cell.2019.05.031.

85. Bergen, V., Lange, M., Peidli, S., Wolf, F.A., and Theis, F.J. (2020). Generalizing RNA velocity to transient cell states through dynamical modeling. Nat. Biotechnol. *38*, 1408–1414. https://doi.org/10.1038/s41587-020-0591-3.

86. Trapnell, C., Cacchiarelli, D., Grimsby, J., Pokharel, P., Li, S., Morse, M., Lennon, N.J., Livak, K.J., Mikkelsen, T.S., and Rinn, J.L. (2014). The dynamics and regulators of cell fate decisions are revealed by pseudotemporal ordering of single cells. Nat. Biotechnol. *32*, 381–386. https://doi.org/10.1038/nbt.2859.

87. Langmead, B., Trapnell, C., Pop, M., and Salzberg, S.L. (2009). Ultrafast and memory-efficient alignment of short DNA sequences to the human genome. Genome Biol. *10*, R25. https://doi.org/10.1186/gb-2009-10-3-r25.

88. Langmead, B., and Salzberg, S.L. (2012). Fast gapped-read alignment with Bowtie 2. Nat. Methods *9*, 357–359. https://doi.org/10.1038/nmeth.1923.

89. Zhang, Y., Liu, T., Meyer, C.A., Eeckhoute, J., Johnson, D.S., Bernstein, B.E., Nusbaum, C., Myers, R.M., Brown, M., Li, W., and Liu, X.S. (2008). Model-based analysis of ChIP-Seq (MACS). Genome Biol. *9*, R137. https://doi.org/10.1186/gb-2008-9-9-r137.

90. Ross-Innes, C.S., Stark, R., Teschendorff, A.E., Holmes, K.A., Ali, H.R., Dunning, M.J., Brown, G.D., Gojis, O., Ellis, I.O., Green, A.R., et al. (2012). Differential oestrogen receptor binding is associated with clinical outcome in breast cancer. Nature *481*, 389–393. https://doi.org/10.1038/nature10730.

91. Yunis, J.J., Roldan, L., Yasmineh, W.G., and Lee, J.C. (1971). Staining of satellite DNA in metaphase chromosomes. Nature *231*, 532–533. https://doi.org/10.1038/231532a0.

92. Gu, Z., Eils, R., and Schlesner, M. (2016). Complex heatmaps reveal patterns and correlations in multidimensional genomic data. Bioinformatics Oxf. Engl. *32*, 2847–2849. https://doi.org/10.1093/bioinformatics/btw313.

93. Mcinnes, L., Healy, J., Saul, N., and Großberger, L. (2018). UMAP: uniform manifold approximation and projection. J. Open Source Software *3*, 861. https://doi.org/10.21105/joss.00861.

94. Yu, G., Wang, L.G., and He, Q.Y. (2015). ChIPseeker: an R/Bioconductor package for ChIP peak annotation, comparison and visualization. Bioinformatics Oxf. Engl. *31*, 2382–2383. https://doi.org/10.1093/bioinformatics/btv145.

95. Ramírez, F., Ryan, D.P., Grüning, B., Bhardwaj, V., Kilpert, F., Richter, A.S., Heyne, S., Dündar, F., and Manke, T. (2016). deepTools2: a next generation web server for deep-sequencing data analysis. Nucleic Acids Res. *44*, W160–W165. https://doi.org/10.1093/nar/gkw257.

Please cite this article in press as: Huang et al., Inhibition of HDAC activity directly reprograms murine embryonic stem cells to trophoblast stem cells, Developmental Cell (2024), https://doi.org/10.1016/j.devcel.2024.05.009

STAR★METHODS

KEY RESOURCES TABLE

REAGENT or RESOURCE	SOURCE	IDENTIFIER
Antibodies		
Rabbit polyclonal anti-NANOG	Bethyl	Cat#A300-397A-M; RRID: AB_386108
Rabbit monoclonal anti-OCT4	Santa Cruz	Cat#sc-5279; RRID: AB_628051
Rabbit monoclonal anti-SOX2	Cell Signaling Technology	Cat#23064s; RRID: AB_2714146
Mouse monoclonal anti-CDX2	Abcam	Cat#ab76541; RRID: AB_1523334
Goat polyclonal anti-GATA6	R&D systems	Cat#AF1700; RRID: AB_2108901
Mouse monoclonal anti-AP2γ	Abcam	Cat#ab110635; RRID: AB_10858471
Goat Polyclonal anti-mCherry	Arigo	Cat#ARG55723
Goat Polyclonal ant-Podocalyxin	R&D systems	Cat#AF1556; RRID: AB_354858
Rabbit polyclonal anti-GCM1	Antibody online	Cat#ABIN2792608
Alexa Fluor™ 488-Phalloidin	Invitrogen	Cat#A12379
Rabbit monoclonal anti-H3K9ac	Cell Signaling Technology	Cat#9649T
Rat monoclonal anti-SOX2	Invitrogen	Cat#14-9811-82; RRID: AB_11219471
Rabbit monoclonal anti-H3K27ac	Cell Signaling Technology	Cat#8173s; RRID: AB_10949503
Rabbit monoclonal anti-H3	Cell Signaling Technology	Cat#4499s; RRID: AB_10544537
Rabbit polyclonal anti-ZMYM2	Thermo Fisher Scientific	Cat#PA5-28265; RRID: AB_2545741
FITC Annexin V	BD Biosciences	Cat# 556420
Rabbit polyclonal Anti-mCherry antibody	Abcam	Cat#ab167453; RRID: AB_2571870
Rat monoclonal Alexa Fluor® APC anti-CD40	Invitrogen	Cat#17-0401-82; RRID: AB_469385
Rat monoclonal Alexa Fluor® APC anti-CD140a	Invitrogen	Cat#17-1401-81; RRID: AB_529482
Donkey polyclonal anti-Goat IgG (H+L) Highly Cross-Adsorbed, Alexa Fluor Plus 488	Invitrogen	Cat#A32814; RRID: AB_2762838
Donkey polyclonal anti-Rabbit IgG (H+L) ReadyProbes™, Alexa Fluor 488	Invitrogen	Cat# R37118; RRID: AB_2556546
Donkey polyclonal anti-Mouse IgG (H+L) Highly Cross-Adsorbed, Alexa Fluor 488	Invitrogen	Cat#A32766; RRID: AB_2762823
Donkey polyclonal anti-Goat IgG (H+L) Cross-Adsorbed, Alexa Fluor 568	Invitrogen	Cat#A11057; RRID: AB_2534104
Donkey polyclonal anti-Mouse IgG (H+L) Highly Cross-Adsorbed, Alexa Fluor 647	Invitrogen	Cat#A31571; RRID: AB_162542
Donkey polyclonal anti-Rabbit IgG (H+L) Highly Cross-Adsorbed, Alexa Fluor 647	Invitrogen	Cat#A31573; RRID: AB_2536183
Bacterial and virus strains		
pLVX-U6-shRNA-PGK-Puro	MiaoLing Biology	Cat#G6163
psPAX2	The Jing Liu Laboratory (Guangzhou Institutes of Biomedicine and Health, Chinese Academy of Science)	N/A
pMD2.G	The Jing Liu Laboratory (Guangzhou Institutes of Biomedicine and Health, Chinese Academy of Science)	N/A
Chemicals, peptides, and recombinant proteins		
Leukemia Inhibitory Factor (LIF)	Merck	Cat#ESG1107
Sodium butyrate	Sigma-Aldrich	Cat#B5887
Trichostatin A (TSA)	Selleck Chemicals	Cat#S1045
Entinostat (MS275)	Selleck Chemicals	Cat#S1053
Mocetinostat (MGCD0103)	Selleck Chemicals	Cat#S1122

(*Continued on next page*)

Please cite this article in press as: Huang et al., Inhibition of HDAC activity directly reprograms murine embryonic stem cells to trophoblast stem cells, Developmental Cell (2024), https://doi.org/10.1016/j.devcel.2024.05.009

Continued

REAGENT or RESOURCE	SOURCE	IDENTIFIER
TMP195	Selleck Chemicals	Cat#S8502
LMK235	Selleck Chemicals	Cat#S7569
TH34	Selleck Chemicals	Cat#S8773
Tubacin	Selleck Chemicals	Cat#S2239
Progesterone	Sigma-Aldrich	Cat#P0130
β-Estradiol	Sigma-Aldrich	Cat#E2758
Y-27632	Reagents Direct	Cat#53-B80-50
CHIR99021	Reagents Direct	Cat#27-H76
SB431542	Selleck Chemicals	Cat#S1067
Valproic acid	Selleck Chemicals	Cat#S3944
BMP4	Proteintech	Cat#HZ-1040
A83-01	Axon Medchem	Cat#1421
ITS -X	Gibco	Cat#51500056
Recombinant Human FGF-4 (aa 71-206) Protein	R&D systems	Cat#7460-F4-025
Heparin sodium salt from porcine intestinal mucosa	Sigma-Aldrich	Cat#H3149-500KU-9
Critical commercial assays		
Chromium Next GEM Single Cell 3′ GEM, Library & Gel Bead Kit v3.1	10x Genomics	Cat#1000121
EZ-Magna ChIP A/G	Merck Millipore	Cat#17-10086
NEBNext Ultra II DNA Library Prep Kit For Illumina	NEB	Cat#E7645S
NEBNext Multiplex Oligos for Illumina	NEB	Cat#E7335S
TotalPrep™ RNA Amplification Kit	Illumina	Cat#RS-122-2103
PrimeScript™ II Reverse Transcriptase kit	TAKARA	Cat#2690A
TB Green® Premix Ex Taq™ Kits	TAKARA	Cat#RR420
Deposited data		
scRNA-seq, bulk RNA-seq and ChIP-seq data	This study	GEO: GSE193087
RNA-seq data of ESCs and TSCs	Cambuli et al.[9]	GEO: GSE62149
ChIP-seq data of LSD1 and HDAC1/2 in ESCs	Whyte et al.[44]	GEO: GSE27841
scRNA-seq data of E4.5 blastocysts	Nowotschin et al.[74]	GEO: GSE123046
scRNA-seq of EPS cells induced blastoids	Li et al.[48]	GEO: GSE135701
scRNA-seq of TPS cells induced blastoids	Xu et al.[56]	GEO: GSE183522
Original pictures of Western blot	This study	boyan, huang (2024), "DC WB original data", Mendeley Data, V1, https://doi.org/10.17632/kkfhghm4fn.1
Experimental models: Cell lines		
Mouse: E14Tg2a ESC cells	ATCC	Cat#CRL-1821
Mouse: E14Tg2a Hdac1/2 CKO cell line	The Shaun M. Cowley Laboratory (University of Leicester)	N/A
Mouse: OGTS cell line	The Tilo Kunath Laboratory (University of Edinburgh)	N/A
Oligonucleotides		
Primers for RT-PCR, see Table S5	This paper	N/A
Primers for shRNA, see Table S5	This paper	N/A
sgRNA for *Dux*/*Zmym2* knockout cell line, see Table S5	This paper	N/A
Primers for Elf5/Tead4 methylation, see Table S5	This paper	N/A
Primers for Hdac1/2 and their point mutants rescued cell lines Construction, see Table S5	This paper	N/A

(*Continued on next page*)

Please cite this article in press as: Huang et al., Inhibition of HDAC activity directly reprograms murine embryonic stem cells to trophoblast stem cells, Developmental Cell (2024), https://doi.org/10.1016/j.devcel.2024.05.009

Continued

REAGENT or RESOURCE	SOURCE	IDENTIFIER
Recombinant DNA		
PyCAG-mCherry-MERVL-GFP	This paper	N/A
PyCAG-mCherry-Null-GFP	This paper	N/A
SgRNA-Dux-F-eSpCas9(1.1)-T2A-EGFP	This paper	N/A
SgRNA-Dux-R-eSpCas9(1.1)-T2A-EGFP	This paper	N/A
SgRNA-Zmym2-F-eSpCas9(1.1)-T2A-EGFP	This paper	N/A
SgRNA- Zmym2-R-eSpCas9(1.1)-T2A-EGFP	This paper	N/A
pLVX-U6-Lsd1 (mouse) -shRNA1-PGK-EGFP-E2A-Puro	This paper	N/A
pLVX-U6-Lsd1 (mouse) -shRNA2-PGK-EGFP-E2A-Puro	This paper	N/A
PB-Tet-on-Hdac1-PGK-Hygro	This paper	N/A
PB-Tet-on-Hdac1 (H141A)-PGK-Hygro	This paper	N/A
PB-Tet-on-Hdac2-PGK-Hygro	This paper	N/A
PB-Tet-on-Hdac2 (H142A)-PGK-Hygro	This paper	N/A
PB-Tet-on-Dux-PGK-Hygro	This paper	N/A
Software and algorithms		
ImageJ	Schneider et al.[75]	https://imagej.nih.gov/ij/
Graphpad	N/A	https://www.graphpad.com/
FastQC (v0.11.9)	N/A	https://www.bioinformatics.babraham.ac.uk/projects/fastqc/
HISAT2 (v2.2.1)	Kim et al.[76]	http://daehwankimlab.github.io/hisat2/
StringTie (v2.1.5)	Pertea et al.[77]	https://ccb.jhu.edu/software/stringtie/
ComBat-seq	Zhang et al.[78]	https://github.com/zhangyuqing/ComBat-seq
limma	Ritchie et al.[79]	https://bioconductor.riken.jp/packages/3.9/bioc/html/limma.html
trimmomatic (v0.39)	Bolger et al.[80]	https://github.com/usadellab/Trimmomatic
STAR (v2.7.5a)	Dobin et al.[81]	https://github.com/alexdobin/STAR
htseq-count (v0.13.5)	Anders et al.[82]	https://htseq.readthedocs.io/en/master/index.html
DESeq2	Love et al.[83]	https://bioconductor.org/packages/release/bioc/html/DESeq2.html
Cell Ranger (v3.1.0)	10x Genomics	https://www.10xgenomics.com/cn/support/software/cell-ranger
Seurat (v3.2.3)	Stuart et al.[84]	https://satijalab.org/seurat/
Scvelo (v0.2.4)	Bergen et al.[85]	https://scvelo.readthedocs.io/en/stable/index.html
Monocle 2 (v2.14.0)	Trapnell et al.[86]	http://cole-trapnell-lab.github.io/monocle-release/
Bowtie (v1.3.1)	Langmead et al.[87]	https://bowtie-bio.sourceforge.net/index.shtml
Bowtie2 (v2.4.2)	Langmead and Salzberg[88]	https://bowtie-bio.sourceforge.net/bowtie2/index.shtml
MACS2 (v2.2.7.1)	Zhang et al.[89]	https://pypi.org/project/MACS2/
DiffBind (v2.14.0)	Ross-Innes et al.[90]	https://bioconductor.org/packages/release/bioc/html/DiffBind.html

RESOURCE AVAILABILITY

Lead contact

Further queries and reagent requests may be directed and will be fulfilled by the lead contact, Man Zhang (zhang_man@gzlab.ac.cn).

Materials availability

All unique/stable reagents generated in this study are available from the lead contact with a completed Materials Transfer Agreement.

Data and code availability

- All raw sequencing data can be accessed at NCBI Gene Expression Omnibus (GEO) (accession number: GSE193087). Raw count of scRNA-sequencing data of E1.5-E7.5 blastocyst (in house data) can be found in Table S7. The original pictures of the Western blot was uploaded to Mendeley Data (https://doi.org/10.17632/kkfhghm4fn.1).
- This paper does not report original code.
- Any additional information required to reanalyze the data reported in this work paper is available from the lead contact upon request.

EXPERIMENTAL MODEL AND STUDY PARTICIPANT DETAILS

Mice

Animal experiments were performed in compliance with the Guide for the Care and Use of Laboratory Animals published by the National Research Council and approved by Institutional Animal Care and Use Committee of Guangzhou Institutes of Bio-medicine and Health (GIBH) and the Guangzhou National Laboratory. Mice were purchased from HUNAN SJA LABORATORY ANIMAL CO., LTD. and housed in a 12 h light/dark cycle environment in a temperature control room with water and food.

Cell lines

Mouse embryonic stem cell lines were employed for this study. *Hdac1/2* CKO mouse ES cell line was kindly shared by Dr. Shaun M. Cowley (University of Leicester). 2C::GFP reporter cell lines, the *Zmym2* and *Dux* knockout cell lines and rescued cell lines were generated in house. E14Tg2a was employed to generate mCG and mCMG cell lines. MCMG cells, clone 1 (mCMG1) was used to generate *Zmym2* and *Dux* knockout cell lines and doxycycline inducible cell lines. OGTS was kindly shared by Dr. Tilo Kunath (University of Edinburgh). MG1-TS C1 and C2 were generated in house from mCMG ES cell lines. ESCs were cultured in DMEM 4,500 mg/L glucose (SH30022.01, Gibco), 110 mg/l sodium pyruvate (11360070, Gibco), 4 mM L-glutamine (Gibco), 15% fetal bovine serum (10099141, Gibco), 1 U/ml penicillin (15070063, Gibco), 1 mg/ml streptomycin (15070063, Gibco), 0.1 mM nonessential amino acids (11140050, Gibco), 50 mM β-mercaptoethanol (63689, Sigma), and 1000 U/ml LIF (ESG1107, Merck) and maintained in a 37°C humidified incubator with 5% CO_2.

METHOD DETAILS

TSC induction

For TSC induction, ESCs were dissociated and suspended at 3×10^4 cells/ml in ESC medium (DMEM 4,500 mg/l glucose (SH30022.01, Gibco), 110 mg/l sodium pyruvate (11360070, Gibco), 4 mM L-glutamine (Gibco), 15% fetal bovine serum (10099141, Gibco), 1 U/ml penicillin (15070063, Gibco), 1 mg/ml streptomycin (15070063, Gibco), 0.1 mM nonessential amino acids (11140050, Gibco), 50 mM β-mercaptoethanol (63689, Sigma), and 1000 U/ml LIF (ESG1107, Merck)). 3×10^5 cells were plated into one well of the 6-well culture dish (Corning, 3516) with the addition of 0.5 mM sodium butyrate (B5887, Sigma) for 2 days. Cells were then digested with 0.05% trypsin (25200072, Invitrogen). 5×10^4 cells were resuspended by 1×TSC medium (RPMI1640 (72400-047, Gibco), 110 mg/l sodium pyruvate, 20% fetal bovine serum, 0.4 U/ml penicillin, 0.4 mg/ml streptomycin, 50 mM β-mercaptoethanol, 25 ng/ml FGF4 (235-F4-025, R&D system) and 1 μg/ml heparin (H3149, Sigma)) with 0.5 mM NaB and transferred to a new 6-well plates (3516, Corning) coated with irradiated MEF cells. The medium was changed every two days. After 4 days of incubation, cells were digested and 1×10^4 cells were resuspended by 1.5×TSC medium (37.5 ng/ml FGF4 and 1.5 μg/ml Heparin) with 0.5 mM NaB and transferred to another 6-well with MEF cells, continue cultured for 4 to 6 days, and changed the medium every two days (NaB treatment should not last over 12 days in total, otherwise the proportion of iTSCs with abnormal karyotype might increase). Then the clones with TSC morphology were picked up and dissociated with 0.05% trypsin for 5 minutes. The cells were then transferred into a well of the 4-well plate and cultured in 1×TSC medium without NaB. For a successful induction, it is crucial to use fresh FGF4 and heparin with high purity. The inhibitors and their concentration used during the experiments are listed in Table S6.

Establishment of XEN-like cell line

ESCs were treated in the same manner as the TSC induction (described above). At the day 8 of induction, cells were collected and resuspended in 100 μl of PBS/10% FBS buffer supplemented with a 1:100 diluted CD140a antibody (17-1401-81, Invitrogen). After a 20-minute incubation at room temperature, the cells were washed twice in 1 ml of PBS/2% knockout serum (KSR, A3181501, Invitrogen), resuspended in PBS/2% KSR solution, and then filtered using a 35 μm strainer cap. Subsequently, the APC-CD140a-positive cells were sorted using a BD FACXAria III (BD). The CD140a-positive cells were cultured in XEN medium (RPMI 1640 supplemented with 15% FBS, 0.1 mM β-mercaptoethanol, 1% penicillin-streptomycin, 25 ng/ml FGF4 and 1 μg/ml heparin) in a six-well coated with irradiated MEF cells. The cells were passaged every two or three days. The information of inhibitors and cytokines used during the experiments are listed in Table S6.

Please cite this article in press as: Huang et al., Inhibition of HDAC activity directly reprograms murine embryonic stem cells to trophoblast stem cells, Developmental Cell (2024), https://doi.org/10.1016/j.devcel.2024.05.009

Lentiviral-shRNA constructions

The *Lsd1* shRNA (5'-GGAATCGCACATTGCAGTTAT-3' and 5'-GGTTGTCATTCAGCTGCAAGA-3') was designed and ligated into pLVX-U6-shRNA-PGK-Puro vector (G6143, Miaoling). All shRNA plasmids were confirmed by sequencing. HEK293T cells were transfected with three plasmids listed below to produce Lenti-virus. The three plasmids pLKO–shRNA construct(s), pMD2.G, and psPAX2 (donated from Dr. Jing Liu' s lab) were mixed at a ratio of 5:3:2 and transfected into HEK293T cells with Lipo3000 (L3000-05, Invitrogen). The supernatant containing the lentiviral particles was harvested after 48 h transfection. Then, the supernatant was used to infect the E14Tg2a ESCs. The cells expressing the target shRNA were selected by incubation with 2 μg/ml puromycin (A1113803, Gibco). The stable cell lines were used in this study as *Lsd1* knockdown cell line.

Establishment of *Hdac1* and *Hdac2* inducible rescued cell lines

The coding sequences (CDS) of *Hdac1* and *Hdac2* were amplifying from ESC cDNA. The primers (*Hdac1/2*-F/R) are listed in Table S5. The PCR products were then cloned into a transposable vector with a doxycycline-inducible promoter (PB-Tet-on-*Hdac1/2*-PGK-Hygro) by Gibson assembly (2X MultiF Seamless Assembly Mix, RK21020, ABclonal). For the HDAC1/2 point mutation, sequences were amplified by the primers with the point mutation together with the *Hdac1/2*-F/R from the *Hdac1/2* CDS and Gibson cloned into the vector. Their coding sequences were then confirmed by the clonal sequencing. Subsequently, PB-HDAC1/2 with PBase or PB-HDAC1(H141A)/HDAC2(H142A) with PBase were transfect into *Hdac1/2* conditional knockout cell line (a kind gift from Dr. Shaun M. Cowley) by Lipo3000 (L3000015, Invitrogen) at a ratio of 1.5:1.5:1. The cells were then selected with hygromycin (100 μg/ml) for 7 days to obtain stable rescued cell lines.

Immunostaining

Embryos or cells were fixed with 4% paraformaldehyde (PFA, MA0192, Meilunbio) for 30 min at room temperature. Then, samples were washed three times for 5 min in PBS (SH30028.02, HyClone)/0.1%Triton-X100 (T824275, Macklin) (PBST). After permeabilization with PBS/0.3% Triton-X100 for 30 min, samples were blocking by 3% donkey serum (D9663, Sigma) / 1% BSA (Sigma)/ PBST solution for 2 h, embryos were then incubated with the primary antibodies, which are listed in the Table S6, overnight at 4°C. After washing with PBS/0.1%Triton-X100 four times for 5 min each, embryos or cells were incubated with the fluorescent labeled secondary antibodies at room temperature for 2 h. After finished the incubation, embryos or cells were washed and stained with DAPI (D9542, Sigma) for 5 min. Imaging occurred on a Carl Zeiss LSM800 confocal microscope (LSM800, Carl Zeiss) and images were processed using ZEN software (Carl Zeiss). The antibodies used during the experiment are listed in Table S6.

Immunostaining of paraffin sections

For the placentas, and sesame oil- or blastoid-induced deciduae, tissues were fixed with 4% paraformaldehyde (PFA, MA0192, Meilunbio) at room temperature, then send to Servicebio company (Wuhan, China) for paraffin section. Sections were dewaxed, rehydrated, and permeabilized with 0.5% Triton X-100 (T824275, Macklin) for 15 min. Sections were retrieved by boiling in 0.01 M Tris-EDTA (pH=9.0) for 20 min. Subsequently, sections were incubated with 3% donkey serum (D9663, Sigma) / 1% BSA (Sigma)/ PBST solution for 2 h at room temperature, then incubated with the primary antibodies overnight at 4°C. Next day, sections were washed in PBS (SH30028.02, HyClone) three times for 10 min each. Subsequently, sections were incubated with the fluorescent labeled secondary antibodies at room temperature for 2 h. After finished the incubation, sections were washed in PBS three times for 10 min each, and stained with DAPI (D9542, Sigma) for 5 min, and seal section with anti-fluorescent quencher (BL701A, Biosharp). Imaging occurred on a Carl Zeiss LSM800 confocal microscope (LSM800, Carl Zeiss) and images were processed using ZEN software (Carl Zeiss). The antibodies used in the experiments are listed in Table S6.

Karyotype analysis

Chromosome preparations were made in a standard protocol.[91] When cells were grown with 60% confluence, 0.2 μg/ml colchicine (A600322, Sangon Biotech) was added into the medium and treated at 37°C for 130 min. Subsequently, cells were digested by 0.25% trypsin, and treated with 0.075 mol/l KCL (A501159, Sangon Biotech) at 37°C for 28 min. After centrifuge at 1200 rpm/min for 5 min, cells pellets were mixed and incubated in fixative solution (methanol: glacial acetic acid=3:1) at 37°C for 40 min. The cell suspension was then dropped on the slide and oven baken at 75°C for 3 h. Afterwards, slides were incubated in the 0.25% trypsin for 10 s, and the trypsinization was terminated by normal saline. Slides were then stained by Giemsa dye solution for 10 minutes, and dry at room temperature. Images were captured by Carl Zeiss imager Z2 (Carl Zeiss) and processed using Ikaros karyotyping system (MetaSystems).

Flow cytometry (FACS)

Cells were dissociated with 0.05% trypsin and neutralized in the MEF medium (DMEM 4,500 mg/l glucose, 4 mM L-glutamine, 10% fetal bovine serum, 1 U/ml penicillin, 1 mg/ml streptomycin,). Then, the cells were collected by centrifugation and the pellets are re-suspended in 100 μl PBS/10% FBS supplemented with 1: 100 diluted Alexa Fluor® APC anti-CD40 (17-0401-82, Invitrogen). After 30 minutes incubation on ice, the cells were washed twice in 1 ml PBS/2% knockout serum (KSR, A3181501, Invitrogen), resuspended in PBS/2% KSR solution and filtered with 35 μm strainer cap before analysis on a BD LSR Fortessa X-20 (BD). Data were analyzed with FlowJo 10.

Please cite this article in press as: Huang et al., Inhibition of HDAC activity directly reprograms murine embryonic stem cells to trophoblast stem cells, Developmental Cell (2024), https://doi.org/10.1016/j.devcel.2024.05.009

SDS–PAGE electrophoresis and immunoblotting

Cells were washed once with PBS and lysed with RIPA lysis buffer (P0013, Beyotime) which containing 50 mM Tris-HCl (pH 7.4), 150 mM NaCl, 0.1% SDS, 1 mM EDTA, 1% Triton X-100 and fresh-added 1×protease inhibitor cocktail. The concentration of protein in the samples were detected with the BCA protein assay kit (P0012S, Beyotime). 10 μg proteins of each sample were used as a loading content by 10% SDS-PAGE and transferred sample and marker to PVDF membrane (IPVH00010, Millipore). The membranes were blocked with 5% skim milk powder in TBST for 1.5 h at room temperature and incubated overnight at 4°C with primary antibodies, which are listed in Table S6. After incubation, membranes were washed with TBST for 10 mins (three times), and incubated with secondary antibodies (1:5000; Cell Signaling Technology). Membranes were washed with TBST for 10 min (three times), and the bands were visualized by enhanced chemiluminescence using ECL (P0018FS, Beyotime) and captured on Molecular Imager Gel Doc XR$^+$ (Bio-Rad). The original data of the Western blot was uploaded to Mendeley Data, the link can be found in the key resources table (https://doi.org/10.17632/kkfhghm4fn.1).

RNA and qRT-PCR analysis

Total RNA was extracted using Eastep® Super Total RNA Extraction Kit (LS1040, Promega) following the manufacturer's instructions. Reverse transcription reactions were performed using PrimeScript™ II Reverse Transcriptase kit (2690A, TAKARA) and quantitative PCR performed using TB Green® Premix Ex Taq™ Kits (RR420, TAKARA) on QuantStudio™ 7 Flex (ThermoFisher Scientific). Values for each gene were normalized to the expression of TATA-box Binding Protein (TBP) according to $2^{-\Delta CT}$ formula. Oligonucleotide sequences are shown in Table S5.

Bisulfite sequencing

Genomic DNA of ESC, MG1-TS C1, MG1-TS C2, and OGTS were extracted using the TIANamp Genomic DNA Kit (TIANGEN, DP210831). Subsequently, the genomic DNA was subjected to bisulfite treatment using the EpiArt DNA Methylation Bisulfite Kit (EM101, Vazyme), then the DNA was used as a template for amplifying the regions containing CpG site. The bisulfite primer seeker (http://www.zymoresearch.com/pages/bisulfite-primer-seeker) was utilized to design optimal primers for the target regions. The primers are listed in Table S5. The PCR products were extracted by Gel and PCR Clean-up kit (740609, NucleoSpin), and ligated into the T vectors by using Hieff Clone Zero TOPO-TA Cloning Kit (10907ES20, YEASEN), then transfected into DH5α competent cells. Clones were then picked up and sent for sanger sequencing.

Blastoids generation

E14Tg2a and mCMG ESCs were treated as previously described. At day 8 of TSC induction, cells were digested into single cells using 0.1% Trypsin, then flow cytometry was used to remove MEF cells. Then, 2.0×10^4 cells per well were seed into a 24-well AggreWell plate (Stemcell Technologies, 34415) in the medium for the generation of blastoids supplemented with 10 μM Y-27632 (S1049, Selleck), and cultured in the incubator. After 24 h, the medium was removed and replaced with fresh blastoids medium without Y-27632, then the medium was refreshed every two days. At day 5 to day 7, the blastoids were collected using a 1 ml pipette, and picked up using a mouth pipette. Two types of blastoids medium were made following the published formulation.[48,54] EPS-blastoid basal medium is composed of 25% TSC basal medium: RPMI 1640 (11875-093) supplemented with 20% FBS (16000-044), 1% GlutaMAX (35050-061), 1% Sodium pyruvate (11360-070), and 0.1 mM 2-mercaptoethanol (21985-023), all from Thermo Fisher Scientific, 25% N2B27 basal medium: 1:1 mixture of DMEM/F-12 (11330-032) and Neurobasal (21103-049) supplemented with 0.5% N2 (17502-048), 0.5% B27 (17504-044), 1% NEAA (11140-050), 1% GlutaMAX (35050-061), 0.1 mM 2-mercaptoethanol (21985-023), and 5% KnockOut Serum Replacement (Optional, 10828-028), all from Thermo Fisher Scientific), and 50% M16 (Sigma, M7292). Before using, supplemented with 2 μM ROCK inhibitor Y-27632 (Reagents Direct, 53-B80-50), 12.5 ng/ml FGF4 (R&D, 235F4025), 0.5 μg/ml Heparin (Sigma-Aldrich, H3149), 3 μM CHIR99021 (Reagents Direct, 27-H76), 5 ng/ml BMP4 (Proteintech, HZ-1040), and 0.5 μM A83-01 (Axon Medchem, 1421). iBlastoids medium consisted of a 2:1:1 mixture of IVC1 medium, Blastoids basal medium 1 and Blastoids basal medium 2, supplemented with 0.9 μM CHIR99021 (S1263, Selleck), 1 μM SB431542 (S1067, Selleck), 0.5 μM A83-01 (S7692, Selleck), 0.8 mM valproic acid (S3944, Selleck), 10 ng/ml BMP4 (314-BP-010, R&D) and 50 ng/ml EGF (PMG8041, Invitrogen). Blastoids basal medium 1 consisted of a 1:1 mixture of DMEM/F-12 and neurobasal medium, supplemented with 1% B27 supplement (17504044, Gibco), 0.5% N2 supplement (17502048, Gibco), 0.1 mM β-mercaptoethanol, and 1% penicilin-streptomycin. Blastoids basal medium 2 consisted of DMEM/F-12 supplemented with 0.2% FBS, 0.3% bovine serum albumin (A8412, Sigma), 1% ITS-X supplement, 1.5 μg/ml L-ascorbic acid (A92902, Sigma), 0.1 mM β-mercaptoethanol, and 0.5% penicilin-streptomycin.

In vitro culture of blastocysts and blastoids

Blastocysts and blastocysts-like structures were cultured *in vitro* according to the protocol published previously.[57] Blastocysts were cultured in KSOM medium (MR-107-D, Millipore) until E4.5, and then were transferred into the acidic Tyrode's solution as the zona pellucida gradually disappear. The zona-free blastocysts and the blastoids were washed twice with pre-equilibrated IVC1 medium, and transferred in to a μ-Silde 8-well (80826, ibidi), containing pre-equilibrated IVC1 medium, about 4-15 blastocysts per well, cultured in incubators at 37 °C with 5% CO_2. After 3 days, blastocysts attached to the plate, the medium was switched to IVC2 medium. After 2-4 days, the structures were fixed with 4% PFA for 20 min at room temperature for immunofluorescence staining. IVC1 medium consisted of advanced DMEM/F12 medium (11320033, Gibco), 20% FBS, 2 mM L-glutamine, 1% penicilin-streptomycin, 1% 1×ITS-X (51500056, Gibco), 8 nM β-estradiol (E2758, Sigma), 200 ng/ml progesterone (S1705, Selleck), 25 μM N-acetyl-L-cysteine (S1623,

Selleck). IVC2 medium consisted of advanced DMEM/F12 medium, 30% KSR, 2 mM L-glutamine, 1% penicilin-streptomycin, 1% 1× ITS-X, 8 nM β-estradiol, 200 ng/ml progesterone, 25 μM N-acetyl-L-cysteine.

Embryo manipulation

All procedures related to animals were performed following the ethical guidelines of the Guangzhou National Laboratory. ICR female mice were superovulated by intraperitoneal injection of 7.5 U PMSG followed 48 h later by 7.5 U hCG, then mated with ICR male mice. 18-20 h post hCG injection, the zygote-cumulus complexes were collected by tearing the oviduct. After the hyaluronidase digestion, zygotes were collected and cultured in KSOM (MR-101-D, Millipore) until 4-8 cells stage. Aggregating micro-wells were generated in the bottom of a tissue culture dish using gentle pressure with the aggregation needle (DN-10, BLS), covered with KSOM, overlaid with mineral oil (M8410, Sigma). The zona pellucida of 4-8 cell stage embryos was digested by acidic Tyrode's solution (T1788, Sigma). For cells preparation, MG1-TS C1, C2 and 2C::GFP-positive or negative cells were digested using 0.1% Trypsin, and then transferred into 0.1% gelatin-coated plate and incubated at 37°C for 30 min to allow MEF cells attach to the plate. The supernatant cells were collected. For embryo aggregation, zona-free embryos were placed into each microwell, and 8-10 cells (Cells were incubated on ice for 15-30 min to generate cell clumps) were added into each microwell. The aggregates were cultured for 48 h in incubator at 37 °C, with 5% CO_2. The aggregates were then collected and fixed with 4% PFA for 20 min at room temperature for immunofluorescence staining. For blastocysts injection, approximately 10 MG1-TS C1 or MG1-TS C2 cells were aspirated into an injection pipette and injected into the mouse blastocyst using a piezo-assisted micromanipulator. After injection, approximately 18-20 chimeric embryos were transferred into the uteri of 2.5 dpc pseudopregnant recipient ICR females. Chimeric embryos were dissected at E12.5, and the signal of mCherry was observed under a stereo fluorescence microscope (M205C, Leica).

For the transplantation of blastoids, approximately 18-20 day 5 to day 7 blastoids, 25 μl sesame oil (S905724, Macklin) or 25 μl M2 solution (M7167, Sigma) were transferred into the uteri of 2.5 dpc pseudopregnant recipient ICR females and were then dissected at E7.5.

Bulk RNA-seq

Sorted 2C::GFP-negative cells (ESCs), NaB treated GFP-positive cells (2C-like cells), dissociated OGTS, MG1-TS C1 and C2 cells were washed twice in 1 ml PBS/0.05% BSA. Then, total RNA was isolated using Trizol (15596026, Invitrogen) according to manufacturer's instructions. 100∼300 ng mRNA for each sample was enriched using oligo dT magnetic beads and fragmented into short pieces (200-300 bp) by using Illumina® TotalPrep™ RNA Amplification Kit (RS-122-2103, Illumina) following manufacturer's instructions. The first strand complementary DNA (cDNA) was transcribed from the RNA fragments using random hexamer primers, and second strand cDNA was synthesized in a reaction buffer. Double stranded cDNA was purified with magnetic beads and subjected to end reparation. Integrity and size were checked on an Qsep100 (Qsep100, Bioptic). Lastly, the cDNA libraries were sequenced on the Illumina HiSeq 2500 platform, using 50 bp paired-end sequencing.

ScRNA-seq

Cells at different time points during TSC induction were digested and re-suspended in 100 μl MEF medium, 5 μl of FITC Annexin V (556420, BD) were added into the medium and incubated for 15 mins. Cells were washed twice in 1 ml PBS/0.05% BSA before cell sorting on a BD FACS Aria Fusion. Blastoid were dissociated with TrypLE (12604013, Gibco) for 30 mins and neutralized in the MEF medium. Then, individual cells were sorted on a BD FACS Aria Fusion. The cells were counted using Countess (CellDropFL, Denvoix) and the concentration of single cell suspension was adjusted to 1000 cells/μl. Cells were loaded according to standard protocol of the Chromium Next GEM Chip G Single Cell Kit (1000121, 10x Genomics) in order to capture 5000 cells to 10,000 cells/chip position (V3 chemistry). All the remaining procedures including the library construction were performed according to the standard manufacturer's protocol. Single cell libraries were sequenced on Illumina HiSeqXTen instruments using 150 nt paired-end sequencing.

Chromatin immunoprecipitation assay

ChIP assays were using EZ-Magna ChIP™ A/G kit (Millipore-17-10086). After sample processing, cells were fixed with 1% formaldehyde (252549, Sigma) for 10 min, quenched extra formaldehyde with 125 mM glycine. Cells were then washed twice with ice-cold PBS, and resuspended in 0.5 mL of Cell Lysis Buffer and incubate on ice for 15 minutes. Spin the cell suspension and collected cell nuclei. Isolated nuclei were resuspended in Nuclear Lysis Buffer and sonicated in 450 W output power using a LE220-plus sonicator (Covaris) for 200 cycles with 30% duty factor at 4°C. 2 million cell-equivalent of chromatin (50 μL) was diluted to 450 μL with ChIP Dilution Buffer. Then, specific antibodies (Table S6) and 20 μL Protein A&G magnetic beads were added into the samples and incubated overnight at 4 °C. The DNA were de-crosslinked with 5 M NaCl and proteinase K digestion and purified by a DNA affinity column. 4 μg purified DNA served as template was constructed into sequencing library according to NEBNext® Ultra™ II DNA Library Prep Kit for Illumina® (E7645L, NEB) standard manufacturer's protocol. ChIP DNA libraries were sequenced on Illumina HiSeqXTen instruments using 150nt paired-end sequencing.

Bioinformatics analysis

Bulk RNA-seq analysis

For the characterization of established TSCs, the quality of raw reads was assessed using FASTQC (https://www.bioinformatics.babraham.ac.uk/projects/fastqc/). After removing low-quality reads, clean reads were aligned to the mouse reference genome GRCm38 using HISAT2 with default parameters.[76] Gene expression values in transcripts per million (TPM) were calculated using

Please cite this article in press as: Huang et al., Inhibition of HDAC activity directly reprograms murine embryonic stem cells to trophoblast stem cells, Developmental Cell (2024), https://doi.org/10.1016/j.devcel.2024.05.009

StringTie.[77] The published RNA-seq data set from Cambuli et al.,[9] was downloaded from the NCBI Gene Expression Omnibus (GEO accession number GSE62149). Batch correction for our RNA-seq data set and Cambuli et al. data set was perfromed by using the R package ComBat-seq.[78] The limma voom algorithm from limma package[79] was used to assess the differential gene expression (adjusted P value $\leq$ 0.001). Heatmap was plotted using R package ComplexHeatmap.[92] To extract the differential expressed genes of 2C-like cells and TSCs, basic quality control for raw sequencing reads were performed using FastQC(v0.11.9). Sequencing adaptors and low-quality reads/bases were further removed using trimmomatic (v0.39).[80] Clean reads were then aligned to the mouse reference genome (GRCm38) using STAR (v2.7.5a)[81] and only uniquely mapped reads were retained. Raw counts for each gene were estimated using htseq-count (v0.13.5) from the aligned bam files.[82] To identify 2C- and TSC-specific genes compared with mESC, differentially expressed gene analysis was performed using R package DESeq2 (adjusted p value < 0.05 and fold change > 2).[83]

Single-cell RNA-seq data processing

Raw sequencing data based on 10x Genomics library method were first preprocessed with Cell Ranger pipeline (version 3.1.0) to generate the feature-barcode unique molecular identifier (UMI) count matrix for each sample. We next utilized the 'cellranger aggr' function to combine results of all samples together to get the final UMI count matrix with sequencing depth normalized. The subsequent data analyses were mainly using the Seurat package (version 3.2.3).[84] Low-quality cells with less than 1500 genes or over 20% proportion of UMI counts from mitochondrial genes were removed. Cells with total UMI counts above 50000 were also filtered out to remove potential cell doublets. Genes detected in less than 30 cells were discarded. After filtering, 48675 cells were retained for the down-stream analyses. Briefly, normalization and scaling were performed on the raw count matrix. Top 3000 highly variable genes were selected as input for principal component analysis (PCA). Non-linear dimension reduction using uniform manifold approximation and projection (UMAP)[93] was subsequently performed with top 30 principal components (PCs) as input. Cell type annotation was based on expression of canonical markers.

Single-cell trajectory analysis

We used Scvelo (version 0.2.4)[85] in python to construct the cell trajectory for selected clusters (cluster 1, 3, 4, 6, 9, 10, 11, 12, 14, 15). Spliced/unspliced matrices were created using the STAR (v2.7.5a)[81] with "–soloFeatures Velocyto" parameter, then we used the dynamical model to estimate velocity and transcriptional states. To further explore the main trajectory, clusters along branches that leading to a 2C-like fate or mTSC fate were extracted to reconstruct a refined trajectory using Monocle 2 (version 2.14.0).[86] First, top 2000 differentially expressed genes (mean expression >= 0.1 and empirical dispersion >= 0.3* fitted dispersion) of mESC, 2C-like cell, and mTSC were selected as ordering genes. Next, dimension reduction using DDRTree method was performed on the data. Finally, trajectory was constructed by calling the function 'orderCells'.

Integrated analysis with public scRNA-seq Data

To compare our single-cell data with public datasets, we performed data integration using the Seurat v3 integration workflow. Raw count matrix files were downloaded from Gene Expression Omnibus (GEO) and then subjected to the basic preprocessing including normalization and scaling. Anchors between datasets were identified using 'FindIntegrationAnchors' function implemented in Seurat package. These anchors were then passed to the 'IntegrateData' function to generate the integrated data. Standard workflow was performed for the down-stream analyses including cell clustering and visualization with UMAP. Public datasets used in this study: single-cell RNA-seq data from in-house E4.5 blastocysts, GSE123046;[74] single-cell RNA-seq data of cells from extended pluripotent stem (EPS) cells induced blastoids, GSE135701;[48] single-cell RNA-seq data of cells from totipotent potential stem (TPS) cells induced blastoids, GSE183522.[56]

ChIP-seq data analysis

Raw sequencing reads were first subjected to basic quality control using FastQC (v0.11.9). Sequencing adapters and low-quality reads/bases were removed using Trim Galore (v0.6.4_dev). Clean reads were then aligned to the mouse reference genome (GRCm38) using bowtie2 (v2.4.2, –maxins 2000 –no-unal –no-mixed –no-discordant)[88] for data in this study or using bowtie (v1.3.1, –no-unal -m 1)[87] for public ChIP-seq data (read length=36). Only uniquely mapped reads with mapQ >= 30 were retained. Duplicated reads were also discarded. MACS2 (v2.2.7.1)[89] was used for peak calling (–nomodel –keep-dup all –gsize mm –qvalue 0.05). Differential peak analysis was performed using DiffBind package (v2.14.0, fold change > 1.5, FDR < 0.05).[90] ChIPseeker (v1.22.1) was used for peak annotation.[94] Specially for public data, region of a ChIP targeted gene was defined as the 3kb upstream region of the transcription start site (TSS) and the gene body. BEDTools (v2.29.1) intersect function was used for calculating peak overlap between different datasets, with parameters '-f 0.3 -r'. Normalized ChIP-seq signal (CPM, counts per million mapped reads) was calculated using bamCompare and bamCoverage in deepTools (v3.5.1)[95] for data in this study and public data, respectively. ChIP-seq signal was visualized with IGV genome browser. Binding profiles over region surrounding the TSS of specific genes were generated by computeMatrix and plotProfile function in deepTools. Public datasets used in this study: GSE27841,[44] ChIP-seq data of LSD1 and HDAC1/2 in ESCs.

QUANTIFICATION AND STATISTICAL ANALYSIS

Quantification and statistical analysis were performed using GraphPad Prism 9.0 software. Data are presented as the mean ± SD. The p values were calculated by Student's two-sided paired t-test and indicated in the figures. The p values < 0.05 were considered statistically significant. Statistical methods are indicated in the corresponding figure legends. Hypergeometric test was used to calculate the statistical significance of overlap between different gene sets, as shown in Figures 6C, 6D, and 6F. No methods were used to determine whether the data met assumptions of the statistical approach.